REPORT DOCUMENTATION PAGE

Form Approved
OMB No. 0704-0188

1. REPORT DATE *(DD-MM-YYYY)*	2. REPORT TYPE	3. DATES COVERED *(From - To)*
30-01-2008	Journal Article	

4. TITLE AND SUBTITLE
Role of Minerogenic Particles in Light Scattering in Lakes and a River in Central New York

5a. CONTRACT NUMBER

5b. GRANT NUMBER

5c. PROGRAM ELEMENT NUMBER
0602435N

6. AUTHOR(S)
Feng Peng, Stevel Effler, David O'Donnell, MaryGail Perkins, Alan D. Weidemann

5d. PROJECT NUMBER

5e. TASK NUMBER

5f. WORK UNIT NUMBER
73-6867-06-5

7. PERFORMING ORGANIZATION NAME(S) AND ADDRESS(ES)
Naval Research Laboratory
Oceanography Division
Stennis Space Center, MS 39529-5004

8. PERFORMING ORGANIZATION REPORT NUMBER
NRL/JA/7330-06-6311

9. SPONSORING/MONITORING AGENCY NAME(S) AND ADDRESS(ES)
Office of Naval Research
800 N. Quincy St.
Arlington, VA 22217-5660

10. SPONSOR/MONITOR'S ACRONYM(S)
ONR

11. SPONSOR/MONITOR'S REPORT NUMBER(S)

12. DISTRIBUTION/AVAILABILITY STATEMENT
Approved for public release, distribution is unlimited.

13. SUPPLEMENTARY NOTES

14. ABSTRACT

The role of minerogenic particles in light scattering in several lakes and a river (total of ten sites) in central New York, which represent a robust range of scattering conditions, was evaluated based on an individual particle analysis technique of scanning electron microscopy interfaced with automated x-ray microanalysis and image analysis (SAX), in situ bulk measurements of particle scattering and backscattering coefficients (b_p and b_{bp}), and laboratory analyses of common indicators of scattering. SAX provided characterizations of the elemental x-ray composition, number concentration, particle size distribution (PSD), shape, and projected area concentration of minerogenic particles (PAV_m) of sizes >0.4 •m. Mie theory was applied to calculate the minerogenic components of b_p (b_m) and b_{bp} ($b_{b,m}$) with SAX data. Differences in PAV_m, associated primarily with clay minerals and $CaCO_3$, were responsible for most of the measured differences in both b_p and b_{bp} across the study sites. Contributions of the specified minerogenic particle classes to b_m were found to correspond approximately to their contributions to PAV_m. The estimates of b_m represented substantial fractions of b_p, whereas those of $b_{b,m}$ were the dominant component of b_{bp}. The representativeness of the estimates of b_m and $b_{b,m}$ was supported by their consistency with the bulk measurements. Greater uncertainty prevails for the $b_{b,m}$ estimates than those for b_m, associated primarily with reported deviations in particle shapes from sphericity. The PSDs were well represented by the "B" component of the two-component model or a three parameter generalized....

15. SUBJECT TERMS
light scattering, SAX, particle size distribution

16. SECURITY CLASSIFICATION OF:			17. LIMITATION OF ABSTRACT	18. NUMBER OF PAGES	19a. NAME OF RESPONSIBLE PERSON
a. REPORT	b. ABSTRACT	c. THIS PAGE			Alan D. Weidemann
Unclassified	Unclassified	Unclassified	UL		19b. TELEPHONE NUMBER *(Include area code)* 228-688-6232

Role of minerogenic particles in light scattering in lakes and a river in central New York

Feng Peng,[1,*] Steven W. Effler,[1] David O'Donnell,[1] Mary Gail Perkins,[1] and Alan Weidemann[2]

[1]Upstate Freshwater Institute, P. O. Box 506, Syracuse, New York 13214, USA
[2]Naval Research Laboratory, Stennis Space Center, Mississippi 39529, USA

*Corresponding author: fpeng@upstatefreshwater.org

Received 13 February 2007; revised 11 July 2007; accepted 17 July 2007;
posted 18 July 2007 (Doc. ID 80057); published 7 September 2007

The role of minerogenic particles in light scattering in several lakes and a river (total of ten sites) in central New York, which represent a robust range of scattering conditions, was evaluated based on an individual particle analysis technique of scanning electron microscopy interfaced with automated x-ray microanalysis and image analysis (SAX), *in situ* bulk measurements of particle scattering and backscattering coefficients (b_p and b_{bp}), and laboratory analyses of common indicators of scattering. SAX provided characterizations of the elemental x-ray composition, number concentration, particle size distribution (PSD), shape, and projected area concentration of minerogenic particles (PAV_m) of sizes >0.4 μm. Mie theory was applied to calculate the minerogenic components of b_p (b_m) and b_{bp} ($b_{b,m}$) with SAX data. Differences in PAV_m, associated primarily with clay minerals and $CaCO_3$, were responsible for most of the measured differences in both b_p and b_{bp} across the study sites. Contributions of the specified minerogenic particle classes to b_m were found to correspond approximately to their contributions to PAV_m. The estimates of b_m represented substantial fractions of b_p, whereas those of $b_{b,m}$ were the dominant component of b_{bp}. The representativeness of the estimates of b_m and $b_{b,m}$ was supported by their consistency with the bulk measurements. Greater uncertainty prevails for the $b_{b,m}$ estimates than those for b_m, associated primarily with reported deviations in particle shapes from sphericity. The PSDs were well represented by the "*B*" component of the two-component model or a three parameter generalized gamma distribution [Deep-Sea Res. Part I **40,** 1459 (1993)]. The widely applied Junge (hyperbolic) function performed poorly in representing the PSDs and the size dependency of light scattering in these systems, by overrepresenting the concentrations of submicrometer particles especially. Submicrometer particles were not important contributors to b_m or $b_{b,m}$.

OCIS codes: 120.5820, 180.5810, 290.1350, 290.4020, 290.5850.

1. Introduction

Light scattering by particles is a fundamental regulator of features of radiative transfer within aquatic ecosystems and the emergent flux signal available for remote sensing, and it is important in assessments of physical properties of particles [1]. The magnitude and character of particle scattering are regulated by four features of a particle population: particle number concentration (N), particle size distribution (PSD) [2–4], particle composition [5], and particle shape [6].

The total particle scattering coefficient, $b_p(\lambda)$ (m^{-1}), is defined as

$$b_p(\lambda) = 2\pi \int_0^{\pi} \beta_p(\theta, \lambda) \sin\theta \, d\theta, \tag{1}$$

where λ is the wavelength of the light, $\beta_p(\theta, \lambda)$ is the particle volume scattering function (VSF) describing the angular distribution of the scattered radiation, and θ is the scattering angle; integrating $\beta_p(\theta, \lambda)$ [Eq. (1)] over the angular range from $\pi/2$ to π provides the particle backscattering coefficient, $b_{bp}(\lambda)$. The particle backscattering ratio $\tilde{b}_{bp}(\lambda)$ corresponds

0003-6935/07/266577-18$15.00/0

to $b_{bp}(\lambda)/b_p(\lambda)$. The bulk $\beta_p(\theta, \lambda)$, $b_p(\lambda)$, and $b_{bp}(\lambda)$ are all inherent optical properties (IOPs) of the water medium and therefore are independent of the geometric structure of the light field.

The dependence of $b_p(\lambda)$ and $b_{bp}(\lambda)$ on particle size fractions and compositional components remains uncertain for marine waters [1,7,8], while related information for inland waters is extremely rare [9]. The prevailing opinion for marine systems is that particles larger than 1 μm in size contribute the most to $b_p(\lambda)$ [1], while submicrometer particles (e.g., 0.2 –1 μm) regulate $b_{bp}(\lambda)$ [1,8]. Moreover, minerogenic particles are generally believed to play relatively more important roles in regulating scattering in most case 2 marine waters [1,5,7], and probably in inland waters [9], compared to in case 1 waters, though definitive inorganic particle information has been lacking [8].

IOPs are additive; the total is the sum of the contributing components [10,11], as illustrated here for total scattering, $b(\lambda)$:

$$b(\lambda) = b_p(\lambda) + b_w(\lambda), \tag{2}$$

where $b_w(\lambda)$ and $b_p(\lambda)$ are the scattering coefficients of pure water (seawater for marine systems) and particles, respectively. The magnitude of $b_w(\lambda)$ is small relative to $b_p(\lambda)$ in the vast majority of waters (i.e., $b \approx b_p$). A robust representation would partition $b_p(\lambda)$ into organic $[b_o(\lambda)]$ and minerogenic $[b_m(\lambda)]$ particle components according to

$$b_p(\lambda) = b_o(\lambda) + b_m(\lambda). \tag{3}$$

Stramski *et al.* [7,8] supported a reductionist approach of increased partitioning of IOPs into contributing components to develop improved understanding of the substantial variability in ocean optical properties and its origins. There is adequate evidence, though more circumstantial in nature, that a similar approach would be necessary to understand dynamics within individual freshwater systems [12], as well as differences among systems [13] that are similar to variations among case 2 systems [5]. A reductionist version of Eq. (3) would be

$$b_p(\lambda) = \sum_{i=1}^{N_o} b_{o,i}(\lambda) + \sum_{j=1}^{N_m} b_{m,j}(\lambda), \tag{4}$$

where $b_{o,i}(\lambda)$ is the scattering coefficient of the ith organic particulate component and $b_{m,j}(\lambda)$ is the scattering coefficient of the jth minerogenic particulate component. Application of the reductionist approach by Stramski *et al.* [7] to model scattering, by using multiple particulate components under a variety of hypothetical conditions, yielded insights concerning optical variability in the ocean. Their analysis focused on partitioning the organic particle population, i.e., $b_o(\lambda)$. Twenty-one components were included in the analysis: 18 planktonic (one for viruses, one for heterotrophic bacteria, and 16 phytoplankton groups/species), and one each for detritus, mineral particles, and bubbles. Their speculative model simulations depicted a potentially important role of minerogenic particles in regulating $b_p(\lambda)$ and $b_{bp}(\lambda)$ in both case 1 and case 2 waters.

Advancement of the reductionist approach in partitioning IOPs has been limited by the lack of technologies to quantify light-scattering attributes of multiple particle classes in real ecosystems. While measurements of N and PSDs have been made widely (e.g., Coulter counters [14]), the lack of chemical characterization by these technologies prevents partitioning according to composition. The size threshold of many of these instruments (e.g., ≥1 μm) is also problematic, particularly for the $b_{bp}(\lambda)$ issue [1,8]. Recently, using an individual particle analysis technique, scanning electron microscopy interfaced with automated x-ray microanalysis and image analysis (SAX), Peng and Effler [15] described the light-scattering attributes of minerogenic particles (> 0.2 μm) in a turbid reservoir where these particles dominate $b_p(\lambda)$. SAX provides characterizations of elemental x-ray composition, N, PSD, and shape for multiple geochemical classes of minerogenic particles. "Reasonably good" closure was reported [15] between Mie theory estimates of $b_m(660)$ based on SAX data and measurements of the beam attenuation coefficient at 660 nm $[c(660) \approx 1.045 \times b_p(660)]$ [5].

Here we describe and contrast the light-scattering features of several lakes and a river based on individual particle analyses, *in situ* bulk measurements of $b_p(\lambda)$ and $b_{bp}(\lambda)$, and laboratory analyses of indicators of scattering. We use SAX to characterize the light-scattering attributes of minerogenic particles in these systems and partition this fraction into noteworthy contributing generic type components. Implementations of the forward method in modeling light scattering and of the reductionist approach in partitioning IOPs are advanced through Mie theory calculations of $b_m(\lambda)$ and $b_{b,m}(\lambda)$. The findings are used to evaluate and contrast the role of minerogenic components in regulating features of scattering for the study systems and to estimate $b_o(\lambda)$.

2. Methods

A. Study System

The study systems include five lakes and a 21 km reach of a river located in central New York (Fig. 1). These alkaline hard-water systems represent a substantial range of trophic state and sediment content. All the study lakes stratify in summer, though wide differences in flushing rates prevail among these systems (Table 1). Owasco, Skaneateles, and Otisco Lakes are the easternmost of New York's 11 Finger Lakes. Onondaga Lake, located in metropolitan Syracuse, is polluted by municipal effluent and residual industrial waste [13]. Pelagic lake sites were assessed (Fig. 1), except for a shallow (~3 m) unstratified location in the southern end of Otisco Lake that adjoins the mouth of the largest tributary and is isolated from the main portion of the lake by a constructed causeway.

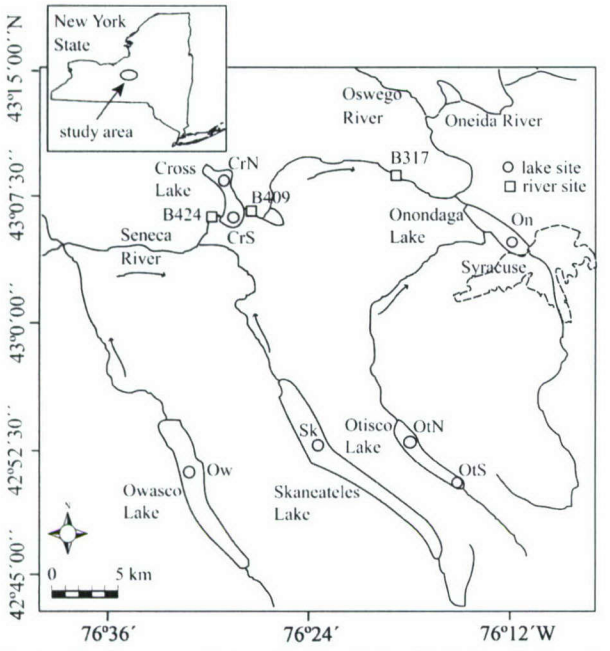

Fig. 1. Study area and sites in central New York. See Table 1 for site abbreviations.

All the study lakes drain into the Seneca River (basin area of 9000 km^2, average flow of 96 m^3 s^{-1}), which, after combining with the Oneida River to form the Oswego River (Fig. 1), enters Lake Ontario. Large sediment and nutrient loads are carried by the river upstream of Cross Lake [16,17]. Cross Lake is an intervening lake for this river (> 95% of inflow to the lake) [16]. Short-circuited flow of the river input to this lake's outflow (i.e., downstream portions of the river), which promotes differences in various characteristics along the lake's primary axis [16], is common. Two sites were assessed in Cross Lake (Fig. 1), one in the northern portion, the second further south and closer to the river inflow. The three river sites (adjoining navigation buoys B424, B409, and B317, Fig. 1) were selected to depict the effects of Cross Lake and *Dreissena polymorpha* (zebra mussels) metabolism, respectively. Dense populations of this bivalve invader prevail between Cross Lake's outflow and the downstream study boundary (between buoys B409 and B317), resulting in substantial changes in common measures of water quality over this reach, including increased clarity [17].

B. Sampling, and Laboratory and Field Measurements

Near surface samples were collected with a submersible pump between 1000 and 1400 h on four days in July 2005. Common indicators of scattering and water quality were measured in the laboratory, including $c(660)$ (10 cm path length transmissometer; C-Star/WET Labs), turbidity (T_n, nepholometric turbidity units (NTUs); Hach Model 2100AN; Clesceri *et al.* [18], total and fixed suspended solids (TSS and FSS; 1.5-μm pore sized Whatman glass fiber filter for TSS, and FSS after 550 °C, i.e., inorganic), and volatile suspended solids (VSS (=TSS − FSS), approximately organic [18]), and chlorophyll *a* (Chl; Parsons *et al.* [19]). TSS is equivalent to suspended particulate matter (SPM), the term commonly adopted in marine studies. To account for the underestimation of FSS due to the structural water loss in clay minerals during the ignition process, a fraction (structural water mass in argillaceous minerals) of 0.09 [20] was used to estimate the water content in the clay-FSS (based on contributions of projected area concentrations of clay particles to that of total mineral particles; see SAX protocols). This water loss was then subtracted from and added to VSS and FSS, respectively, to correct the gravimetrically measured particle concentrations (VSS_{corr} and FSS_{corr}).

T_n and $c(660)$ are surrogate measures of b_p [5,10]. Measurements of $c(660)$ and T_n, and filtering for TSS

Table 1. Characteristics of Study Systems and Location of Sites

System[a] (Abbreviation)	Location[b]		Mean Depth (m)	Surface Area (km^2)	Trophic State[c]	Sampling Date (July)
	Latitude	Longitude				
Owasco L. (Ow)	42° 52′03.35″ N	76° 31′24.50″ W	29.3	26.7	m	28
Skaneateles L. (Sk)	42° 52′05.35″ N	76° 31′24.50″ W	43.5	35.9	o	8
Otisco L.			10.2	7.6	m	
North (OtN)	42° 52′21.24″ N	76° 17′42.10″ W	—	—	—	28
South (OtS)	42° 50′40.77″ N	76° 15′22.33″ W	—	—	—	28
Onondaga L. (On)	43° 06′54″ N	76° 14′34″ W	10.9	12.0	e	27
Cross L.			5.5	9.0	e	
North (CrN)	43° 08′23.47″ N	76° 29′05.94″ W	—	—	—	29
South (CrS)	43° 06′57.01″ N	76° 28′28.67″ W	—	—	—	29
Seneca R.						
B424	43° 06′05.02″ N	76° 29′57.21″ W	—	—	—	29
B409	43° 06′14.18″ N	76° 26′41.19″ W	—	—	—	29
B317	43° 08′49.17″ N	76° 18′50.16″ W	—	—	—	29

[a]See Fig. 1.
[b]World Geodetic System 1984.
[c]o, oligotrophic; m, mesotrophic; e, eutrophic.

and Chl, were conducted on the day of sample collection. Measurements of $c(660)$ were also made *in situ* (same model as laboratory unit) at approximately the time of sampling with profiling instrumentation (SeaBird SeaLogger Profiler). Additionally, spectral absorption, attenuation, and particulate backscattering coefficients [$a(\lambda)$, $c(\lambda)$, and $b_{bp}(\lambda)$] were measured using a combined instrument package (same profiling cage, integrated outputs) of ac-s (spectral absorption and attenuation meter, path length 25 cm) and BB9 (WET Labs, Inc., Philomath, Oregon, USA), also at approximately the time of sampling. The ac-s measures $a(\lambda)$ and $c(\lambda)$ (relative to pure water), and has a spectral resolution of 4 nm over the range of 400–730 nm. The instrument was calibrated according to guidelines of the manufacturer [21] with pure water and checked between deployments by an air calibration protocol. Corrections for differences in pure-water absorption and attenuation due to temperature were made according to Pegau *et al.* [22]. The ac-s absorption spectra were corrected for scattering error through a WET Labs protocol that uses a reference λ to determine the value of the scattering coefficient to be subtracted from $a(\lambda)$. The spectral particulate scattering coefficient, $b_p(\lambda)$, was obtained as the difference, $c(\lambda) - a(\lambda)$. The relative errors for attenuation measurements as a result of multiple scattering (corresponding to optical thickness of <0.8 for the C-Star and <2 for the ac-s) were $<5\%$ [23], with $b_{bp}(\lambda)$ obtained at nine wavelengths (412, 440, 488, 510, 532, 595, 650, 676, and 715 nm) by the BB9 backscattering meter. This instrument measures the VSF at the angle of 117° [$\beta(117°, \lambda)$], an angle identified as a minimum convergence point for variations in $\beta(\theta, \lambda)$ caused by suspended particles and water itself. Corrections for attenuation along the path from the light source to the sample volume to the detector were based on the paired ac-s measurements of $a(\lambda)$, using a protocol described by the manufacturer [24]. Particulate VSF was measured at 117°, $\beta_p(117°, \lambda) = \beta(117°, \lambda) - \beta_w(117°, \lambda)$, the latter being the volume scattering of water. The value of $b_{bp}(\lambda)$ was estimated from the $\beta_p(117°, \lambda)$ according to, $b_{bp}(\lambda) = 2\pi\chi\beta_p(117°, \lambda)$, where the value of χ is 1.1 [25].

C. Scanning Electron Microscopy Interfaced with Automated X-Ray Microanalysis and Image Analysis Protocols

Sample preparation and analytical methods for SAX have been described previously [26,27]; salient features are reviewed here. Particles were deposited onto polycarbonate membranes (25 mm diameter, 0.4 μm pore size) by pressure filtration and carbon coated. SAX was conducted with an Aspex Microanalysis System with Perception Analysis Software (with a plug-in Automated Feature Analysis Module). Approximately 2000 particles were analyzed for each of the ten samples for both elemental and morphometric characteristics. The time required for each analysis was ~3 h. Particles of sizes $>\sim 0.2$ μm are characterized (based on the electron beam search step size), but only those greater than the nominal filter pore size are reported here.

Composition of individual particles is assessed by SAX based on the acquisition of x-ray counts for 16 elements (Na and higher atomic number, including Al, Si, Ca, Fe, Mn). Elemental composition of a particle is represented by its normalized elemental x-ray counts, i.e., relative intensities [28]. Particles were partitioned into eight generic biogeochemical types or classes (Table 2) according to a scheme developed earlier for the Finger Lakes of New York [27]; the definitions of particle types are consistent with the geochemical and mineralogical setting of the region. This classification scheme differs from that used for the low alkalinity (and low $[Ca^{2+}]$) waters of the Catskill region [26] of New York by the inclusion of types for particles containing Ca, consistent with the summertime precipitation of $CaCO_3$ (calcite) that is known to occur in several of the lakes of this study [13]. The "Clay" class corresponds to clay minerals,

Table 2. Specification of Generic Particle Types, According to X-Ray Characteristics, and the Complex Refractive Indices (Relative to Water) Used in Mie Calculations

Type	Description	X-Ray Characteristics	Sources/Origins	m
Organics	Biological	Low x-ray net counts ($\leq$750)[a]	Autochthonous/terrigenous	
Clay	Aluminosilicates	Al, 5 to 55%; Si, 20 to 85%; Al *plus* Si $\geq$ 50%[b]	Terrigenous	1.173–0.001i
Ca-rich	$CaCO_3$ precipitates	Ca $\geq$ 85%	Autochthonous	1.199–0.0001i
Ca-agg	$CaCO_3$ coating on other particles	20% $\leq$ Ca $<$ 85%	Autochthonous/terrigenous	1.186–0.0005i
Quartz	Mineral SiO_2	Si $\geq$ 90%, high x-ray density[c]	Terrigenous	1.155–0.0001i
Diatom	Biogenic SiO_2	Si $\geq$ 90%, low x-ray density[c]	Autochthonous	
Si-rich	Si-containing minerals, silicates	60% $\leq$ Si $<$ 90%	Terrigenous	1.173–0.001i
Other[d]	Miscellaneous particles	Not specified	Various	1.173–0.001i

[a]Live x-ray acquisition time was 3 s.
[b]All percentages are elemental x-ray relative intensities.
[c]The x-ray density refers to the ratio of a particle's total x-ray counts to its size [26].
[d]This incorporates all inorganic particles not captured in the specified classes.

"Quartz" to SiO_2 (mineral phase), and "Si-rich" to other silicate minerals. These classes have terrigenous origins. The "Diatom" and "Quartz" particles were differentiated according to the protocol of Peng *et al.* [26], which is based on the lower x-ray count rates and the larger size of diatoms compared to those of quartz. The "Ca-rich" class corresponds to calcite particles or $CaCO_3$-coated particles, and reflects autochthonous formation in the water columns of the study systems [29]. The "Ca-agg" group represents aggregate particles that have been attributed to the coating of terrigenous particles by calcite precipitation [28]. The "Other" class contains inorganic particles not represented by the specified groups (Table 2).

The "Organics" class systematically underrepresents the contributions of organic particles due to their common composition of low atomic number elements (lower than that of Na), as a result of methodological limitations inherent to SAX [26,28]. Nonetheless, the enumeration of this particle population by SAX and subsequent calculations provide semi-quantitative estimates of its contribution to the overall PAV.

Morphometric characterization of particles by SAX is based on a "rotating chord" algorithm, which provides a detailed representation of morphometries of individual particles [15], including projected area (PA), length, and width. Particle size (d) is calculated from PA as the circular area equivalent diameter. The total projected area concentration (total sample PA per unit volume of water, PAV) is the sum of the individual PA values (result of extrapolation based on the fraction of analyzed filter area) divided by the filtered volume of water sample. PAV can be partitioned into contributing components, e.g., minerogenic PAV (PAV_m), clay-PAV, or other type components as listed in Table 2.

The "nonsphericity" of a particle (e.g., shape factor) is represented by the aspect ratio (ASP), defined as the ratio of a particle's length to its width [30]. A sphere has an ASP value of 1; increases in ASP correspond to greater deviations from spheres. Morphometric features were used to resolve the contribution of *Phacotus* (a phytoplankton with a $CaCO_3$ lorica [27]) to the Ca-rich class, based on its nearly spherical shape (i.e., ASP approaches 1) and large size ($d \geq 8$ μm). This differentiation effectively results in nine delineated particle classes.

D. Particle Size Distributions, Calculations of b_m and $b_{b,m}$, and Estimates of b_o

PSDs are presented as $F(d)$, such that $F(d)\Delta d$ gives the PAV of water in the size range $d \pm 1/2(\Delta d)$ (d is the midpoint and Δd is the width of a size bin). The measured minerogenic PSDs were fitted with two different functional representations, the Junge (or hyperbolic) and the B component of the two-component (2C-B) model. The fitting of the Junge model [$F(d) = Cd^{-j}$, where C is a constant depending on N, and j is the slope of the distribution when linearity is assumed in the log–log plot of $F(d)$], was limited to particles with $d > 1.25$ μm, a typical lower threshold for particle counters [2,31]. Risović's two-component model (TCM) [4,32] is defined as

$$F(d) = C_A d^{\mu_A} \exp(-52 d^{\gamma_A}) + C_B d^{\mu_B} \exp(-17 d^{\gamma_B}), \quad (5)$$

where C_A and C_B are proportional to the number concentrations of small and large particles, respectively, and μ_i and γ_i ($i = A, B$) are parameters of the distribution. In our earlier application of this model, we have found that the B component alone adequately represented the particle sizes (>0.5 μm) responsible for $b_m(660)$ in Schoharie Reservoir, New York, USA [15]; this reduced the number of function coefficients by half, and avoided negative values of C_A when Eq. (5) was fitted to SAX-measured PSD data from the reservoir [15].

The bulk-scattering coefficients for minerogenic particles were calculated, based on the individual particle information from SAX, according to

$$b_m(\lambda) = \sum_{i=1}^{N_m} Q_{bm,i}(m_i, \lambda, d_i) \mathrm{PA}^*_{m,i}, \quad (6)$$

where N_m is the number of minerogenic particles per unit volume of water (number m^{-3}), $Q_{bm,i}$ is the dimensionless efficiency factor for scattering of the ith minerogenic particle with the adjusted projected area of $\mathrm{PA}^*_{m,i}$ (m^2; see subsequent text); likewise, $b_{b,m}(\lambda)$ was calculated with the backscattering efficiency factor, $Q_{bbm,i}$. The values of Q factors depend on the particle's relative (to water) refractive index ($m = n - in'$, where n and n' are the real and imaginary parts of the complex index of refraction, respectively), its size (d_i), and λ. The results are reported for $\lambda = 650$ nm [i.e., $b_m(650)$, $b_{b,m}(650)$], a wavelength for which $b_b(\lambda)$ measurements were made, and close to the reference wavelength (660 nm) adopted by Peng and Effler [15] in similar calculations. Nonminerogenic particles (i.e., those of the Organics and Diatom classes, and the *Phacotus* fraction of the Ca-rich class) were excluded in these scattering calculations.

We calculated $Q_{bm,i}$ and $Q_{bbm,i}$ for individual mineral particles using the Mie theory algorithm (for homogeneous spheres) provided by Bohren and Huffman [33]. Values of n (Table 2) were specified or guided by the listings presented by Kerr and Rogers [34] and Woźniak and Stramski [35]. The value for the Ca-rich class corresponded to that of calcite. The Clay, Si-rich, and Other classes were assigned the value of kaolinite, whereas the Ca-agg class corresponded to the average of kaolinite and calcite. The n' values assigned to the particle types (Table 2) were consistent with the bounds adopted in analyses by Woźniak and Stramski [35], and reflected the assumption of minimal absorption by Ca-rich and Quartz classes compared to the others. The calculated contributions of various size classes of minerogenic particles to the overall estimated scattering are presented in a cumulative format (e.g., [5]). Patterns obtained with functional fits are compared to those based on observations. Sensitivity analyses were conducted (for observed d range of each sample) to depict

the dependence of scattering on n values for three PSD cases: the measured, and two described by the Junge function; values of $b_m(650)$ and $b_{b,m}(650)$ were calculated for these cases of PSD with uniform values of n from 1.05 to 1.25 in increments of 0.05. The two Junge function scenarios corresponded first to the fitted j (for observations $d \geq 1.25$ μm) and second specified $j = 4$.

Adjustments in PA values determined for nonspherical particles by SAX are needed to represent their effective projected area (PA*) within the water column, because of their nonrandom orientation ("lying flat") on the filter [14,15]. A PA*/PA ratio value of 0.87 was reported for quartz dust particles by Proctor and Harris [36], and was adopted in an analysis of light scattering by Jonasz [14]. The light-scattering closure analysis based on SAX observations for Schoharie Reservoir, where clay minerals dominated, supported a PA*/PA value of ~0.7 for those particles [15]. The effect of overestimation of PA on $b_m(650)$ and $b_{b,m}(650)$ was bracketed here by two sets of adjustments: first for particles with ASP values ≥1.5, then that of ≥2.5, adopting a PA*/PA ratio of 0.8. The two ASP thresholds were selected to reflect reasonable upper and lower bound adjustments for the effect. Corresponding adjustments in $d(d^*)$ were made in these Mie theory calculations.

The organic scattering component, $b_o(650)$, was calculated as the difference between the *in situ* measurements of $b_p(650)$ and the SAX-based estimate of $b_m(650)$. Additionally, independent estimates of b_o were based instead of Chl concentration ($b_{o,\mathrm{Chl}}$) using a relationship developed for case 1 waters [37], modified to represent an inverse dependency on λ [38],

$$b_{o,\mathrm{Chl}}(\lambda) = 0.347[\mathrm{Chl}]^{0.766}(660/\lambda)0.97. \quad (7)$$

The average scattering and backscattering efficiencies of the minerogenic particle populations, $\langle Q_{b,m} \rangle$ and $\langle Q_{bb,m} \rangle$, were calculated as the ratios of the estimates of minerogenic scattering (b_m and $b_{b,m}$) to PAV_m (as the sum of measured PA_i, without adjustment). In an analogous manner, average efficiencies were also calculated for the various contributing particle classes.

3. Results

A. Indicators of Light Scattering and Contributing Constituents

Wide differences in light-scattering levels were depicted by the common metrics of water quality for the various study sites (Fig. 2). Values of $c(660)$ and T_n ranged from 0.48 m^{-1} and 0.4 NTU for Skaneateles Lake to 14.7 m^{-1} and 22 NTU for the south site on Otisco Lake [Fig. 2(a)]. These two surrogate metrics of scattering were strongly correlated ($r = 0.97$, $p < 0.01$). Concentrations of TSS ranged from ~0.3 (Skaneateles Lake) to nearly 20 g m^{-3} [south site on Otisco Lake; Fig. 2(b)]. Wide differences in the fraction $\mathrm{FSS}_{\mathrm{corr}}/\mathrm{TSS}$ prevailed, ranging from 0.34 for Onondaga Lake to 0.86 for B424 on the Seneca River;

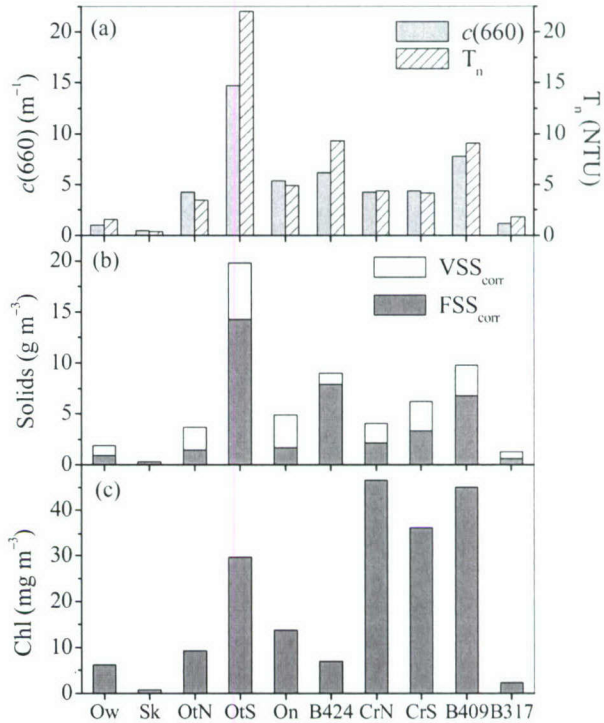

Fig. 2. Bulk water quality metrics for study sites related to light scattering: (a) $c(660)$ and turbidity, (b) suspended solids, and (c) chlorophyll concentration, Chl. See site abbreviations in Table 1.

inorganic components also made large contributions to TSS at the B409 river site and the south site on Otisco Lake. Chl values ranged from 0.7 (Skaneateles Lake) to nearly 50 mg m^{-3} [north site on Cross Lake and B409 on the river; Fig. 2(c)]. Concentrations exceeded 10 mg m^{-3} (i.e., bloom conditions) for five of the ten sites.

Empirical analyses established that TSS was a good predictor of differences in light scattering among the study sites; the linear least-squares regression relationship,

$$c(660) = (0.713 \times \mathrm{TSS}) + 0.613, \quad (8)$$

explained 96% ($p < 0.001$) of the differences in $c(660)$. A similar relationship explained 98% ($p < 0.001$) of the differences in T_n. Relationships to explain the differences in these surrogate metrics of light scattering based on Chl were weak and insignificant. However, a relationship that partitioned the two components of TSS,

$$c(660) = (0.558 \times \mathrm{FSS}_{\mathrm{corr}}) + (1.227 \times \mathrm{VSS}_{\mathrm{corr}}) + 0.105, \quad (9)$$

performed equally well ($r^2 = 0.98$) as the single component representation. The coefficients for both $\mathrm{FSS}_{\mathrm{corr}}$ and $\mathrm{VSS}_{\mathrm{corr}}$ were significant ($p < 0.001$), but the intercept was not. Variations in $\mathrm{FSS}_{\mathrm{corr}}$ explained 88% of the overall variability in $c(660)$; the addition of $\mathrm{VSS}_{\mathrm{corr}}$ explained another 10%. This suggests that differences in the observed light scattering were pri-

marily due to minerogenic particle populations and secondarily to organic particulate components.

B. Composition and Morphometries of Particle Populations

The composition of particle populations is presented in the context of contributions of particle type components to PAV (Table 3) because of the central role this attribute plays in light scattering. The adopted combined geochemical and physical classification scheme performed well in representing the minerogenic particles of these systems, as less than 6% of the PAV was associated with the Other category. PAV_m measurements were strongly correlated ($r = 0.97$) with FSS_{corr} observations. Clay minerals [Fig. 3(a)], $CaCO_3$ [Figs. 3(b) and 3(d)], and $CaCO_3$ aggregates [Fig. 3(a)], common to all the study systems, were the most important minerogenic components. The Clay class was the single largest component of PAV_m at seven of the sites, whereas $CaCO_3$ (non-*Phacotus* component of Ca-rich, together with Ca-agg) was the largest component for the others. Both the Quartz [Fig. 3(a)] and Si-rich classes made smaller contributions. The Clay class made the greatest contribution at B424, upstream of Cross Lake, representing 68.5% and 71.7% of the total and minerogenic PAV, respectively (Table 3). This class made larger contributions to PAV at the south site on Cross Lake, which was closer to the river inflow, than at the north site. The clay mineral PAV and its contribution were much larger at the south shallow site on Otisco Lake than for the north pelagic site. Calcium-containing particle types were the dominant contributors to PAV at the northern site of Otisco Lake (Ca-rich plus Ca-agg, ~58% of PAV; 65% of PAV_m) and Owasco Lake. Diatoms dominated PAV in Skaneateles Lake and were a noteworthy contributor in Cross Lake and in downstream portions of the river. Contributions by *Phacotus* were noteworthy (e.g., >6%) in Cross Lake and the south site on Otisco Lake. The conspicuously higher PAV values for the Organics class for the north Cross Lake and Onondaga Lake sites suggested greater contributions to scattering by organic particles at these locations.

The ASP values for the Diatom class and *Phacotus* fraction of the Ca-rich class present a valuable qualitative context for considering the shape features of the minerogenic particles (Table 4). *Phacotus* [Fig. 3(d)] had a nearly spherical shape, while the diatoms deviated the most from spherical, associated primarily with pennate forms such as *Asterionella* sp. [Fig. 3(c)]. The differences in average ASP values for the diatom populations suggest differences in this community's composition among the study sites. Average ASP values for minerogenic particle classes for all sites were greater than one, depicting deviations from spherical shapes (e.g., Fig. 3). However, these did not approach the much higher values of diatoms. Substantial variability in shape within each minerogenic class was observed at each site, as represented by standard deviations about the mean ASP values (Table 4), but this did not depend on size. The ASP values for the Clay and Ca-agg classes were somewhat higher than for the other minerogenic classes at most of the sites.

Table 3. Summary of PAV Measurements for Study Sites According to Geochemical Classes with Contributions to Total PAV and PAV_m

			Type Contribution (%)								
			Organics				Minerogenic				
			Low X-Ray Counts	Biogenic/Inorganic Coating	Ca-Rich						
System[a]	PAV ($cm^2\ l^{-1}$)	PAV_m ($cm^2\ l^{-1}$)	Organics	Diatom	*Phacotus*	Non-*Phacotus*	Ca-Agg	Clay	Quartz	Si-Rich	Other
Seneca R.											
B424	32.3	30.8 (95.5)[b]	3.2	1.4	0.0	3.6 (3.8)[c]	13.6 (14.2)	68.5 (71.7)	4.4 (4.6)	3.2 (3.4)	2.2 (2.3)
CrN	10.8	5.1 (47.4)	25.4	15.5	11.6	15.3 (32.3)	13.1 (27.7)	9.9 (20.9)	1.1 (2.3)	4.5 (9.5)	3.5 (7.4)
CrS	12.3	8.7 (70.3)	6.9	16.6	6.4	8.5 (12.1)	13.6 (19.3)	35.7 (50.8)	2.0 (2.8)	7.6 (10.8)	2.9 (4.1)
B409	23.2	17.7 (76.6)	8.1	14.8	1.2	3.7 (4.8)	11.2 (14.6)	47.2 (61.6)	4.8 (6.3)	5.0 (6.5)	4.7 (6.1)
B317	3.1	2.4 (77.9)	4.1	18.0	0.0	4.8 (6.2)	6.8 (8.7)	50.5 (64.8)	9.6 (12.3)	2.2 (2.8)	4.0 (5.1)
Lakes											
Ow	2.4	1.9 (78.3)	12.2	6.6	3.0	27.3 (34.8)	14.1 (18.0)	21.3 (27.1)	3.6 (4.6)	6.4 (8.2)	5.6 (7.1)
Sk	2.0	0.43 (21.4)	0.6	78.0	0.0	0.75 (3.5)	2.0 (9.1)	12.4 (58.0)	1.8 (8.6)	1.6 (9.5)	2.8 (13.3)
OtN	7.8	7.0 (89.1)	10.2	0.1	0.6	28.9 (32.4)	29.4 (33.0)	25.7 (28.8)	1.2 (1.3)	1.1 (1.2)	2.8 (7.4)
OtS	50.9	38.3 (75.2)	5.4	10.5	8.8	2.7 (3.6)	5.5 (6.2)	46.7 (62.1)	5.9 (7.8)	8.8 (11.7)	5.61 (7.4)
On	12.3	7.1 (57.7)	41.8	0.5	0.0	6.5 (11.3)	13.1 (22.7)	28.8 (49.9)	2.5 (4.3)	1.8 (3.1)	5.0 (8.7)

[a]See Table 1 for system abbreviations.
[b]Percentages of PAV_m in PAV are listed in parentheses.
[c]Numbers in parentheses are the minerogenic type percentages in PAV_m.

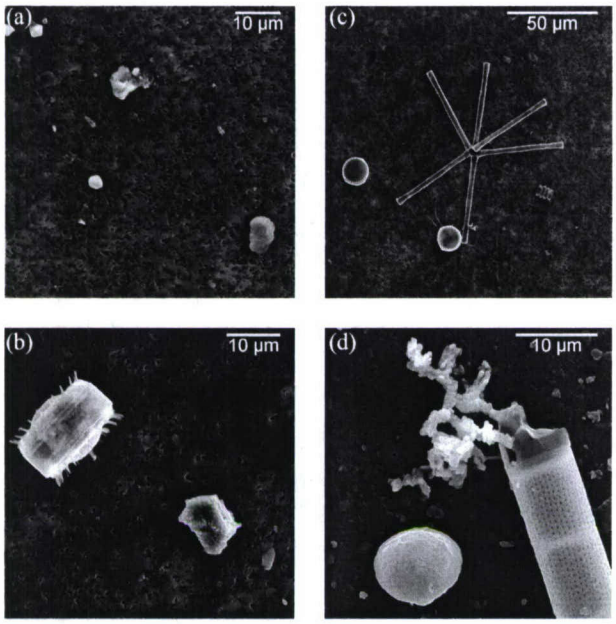

Fig. 3. Micrographs of particles from study sites: (a) Seneca River, quartz ($d \sim 2$ μm) in upper left, clay mineral particles ($d \sim 6$–8 μm) lower right and upper third/left of center, and Ca-agg particle ($d \sim 2$ μm) lower half/left of center, (b) Onondaga Lake, large (>15 μm) centric diatom (on edge) on the left, calcite particle ($d \sim 8$ μm) on lower right, (c) Onondaga Lake, algae, two centric diatoms, a pennate diatom (*Asterionella* sp.) in center, and *Scenedesmus* sp. (Organics) center/right, and (d) Owasco Lake, *Phacotus* sp. ($d \sim 10$ μm) lower left, dendritic calcite particle upper center, and large filamentous diatom (centric) on right.

C. Particle Size Distributions of Mineral Particles

The minerogenic PSDs are presented in two groupings: lake sites [excluding Cross Lake, Fig. 4(a)], and the Cross Lake and Seneca River system [Fig. 4(b)]. The highest particle concentrations occurred at sizes between 0.4 and 0.5 μm, close to the lowest bound of quantification, with the conspicuous exception of the north site on Otisco Lake, where the maximum was at a size of ~1.2 μm [Fig. 4(a)]. Progressive decreases in concentrations were observed for increased particle sizes. Much higher minerogenic N values prevailed throughout the 0.4–10 μm size range at the south Otisco Lake site, compared to the pelagic site in the northern portion of the lake. Similar PSD patterns were observed for Onondaga, Owasco, and Skaneateles Lakes, though substantially higher N levels prevailed in Onondaga [Fig. 4(a)]. Skaneateles Lake had the lowest minerogenic particle concentrations; these were particularly lower than Owasco Lake (next lowest N) for $d > 5$ μm.

Seneca River N levels for $d < 2$ μm were similar upstream (B424) and downstream (B409) of Cross Lake, but were lower for larger (>2 μm) minerogenic particles at the downstream site [Fig. 4(b)]. Higher concentrations were observed at the south site within Cross Lake, which is more proximate to the river inflow, than at the north site. A substantial decrease in minerogenic particle concentrations occurred over the river reach that extends from just downstream of Cross Lake (B409) to a position 18 km further downstream (B317).

None of the minerogenic particle populations characterized here were consistent with a Junge function. Application of this function resulted in overrepresentation of the smaller and larger particles and underprediction of intermediate size particles [an example, the south site of Otisco Lake, is illustrated in Fig. 4(c)]. The values of j ranged from 2.5 to 3.2 (average of 2.8), substantially less than 4, a value commonly invoked in modeling scattering for marine systems [5,35]. The 2C-B performed well ($r^2 > 0.97$ in all fittings) in matching the observed PSDs in the fitted size range (i.e., >0.9 μm), and in most cases this performance extended to smaller sizes [e.g., 0.4–0.5 μm; Fig. 4(c)]. With the exception of the north site of Otisco Lake, values of μ_B and γ_B (Table 5) were similar to the average values (2 and 0.226, respectively) reported by Risović [4] for marine particle populations.

Table 4. Statistics (Mean ± Standard Deviation) of Minerogenic Particle Shapes as Described by ASP (Aspect Ratio) for Study Sites

		Ca-Rich					
System	Diatom	*Phacotus*	Non-*Phacotus*	Ca-Agg	Clay	Quartz	Si-Rich
Seneca R.							
B424	7.4 ± 5.6	—	1.8 ± 0.6	2.4 ± 2.2	2.3 ± 2.8	1.6 ± 1.0	1.7 ± 0.5
Cross L. North	10.1 ± 16.9	1.1 ± 0.1	1.7 ± 0.8	2.3 ± 2.2	2.1 ± 1.2	1.9 ± 1.0	1.8 ± 0.5
Cross L. South	6.6 ± 3.8	1.1 ± 0.1	1.7 ± 0.6	2.1 ± 1.2	2.3 ± 2.0	2.0 ± 1.4	1.7 ± 0.5
B409	7.2 ± 5.6	1.2[a]	1.6 ± 0.5	2.1 ± 1.6	2.2 ± 1.8	1.9 ± 1.6	1.7 ± 0.5
B317	5.7 ± 4.3	—	1.7 ± 0.7	2.0 ± 1.4	1.9 ± 2.0	1.5 ± 0.4	1.6 ± 0.4
Lakes							
Owasco	12.9 ± 13.4	1.2[a]	2.3 ± 2.6	2.6 ± 5.0	2.6 ± 5.4	2.7 ± 2.6	1.8 ± 0.5
Skaneateles	4.1 ± 7.7	—	1.6 ± 0.8	2.1 ± 2.4	2.2 ± 3.0	2.8 ± 2.4	1.7 ± 0.5
Otisco North	3.4 ± 0.7	1.0[a]	2.1 ± 1.7	2.3 ± 1.7	1.9 ± 1.4	1.4 ± 0.3	1.5 ± 0.4
Otisco South	6.0 ± 7.7	1.1 ± 0.0	1.9 ± 1.2	2.2 ± 1.8	2.2 ± 2.1	1.6 ± 0.7	1.6 ± 0.5
Onondaga	9.6 ± 8.4	—	1.5 ± 0.4	2.2 ± 1.6	2.4 ± 2.4	1.6 ± 0.7	1.6 ± 0.4

[a]Less than three observations.

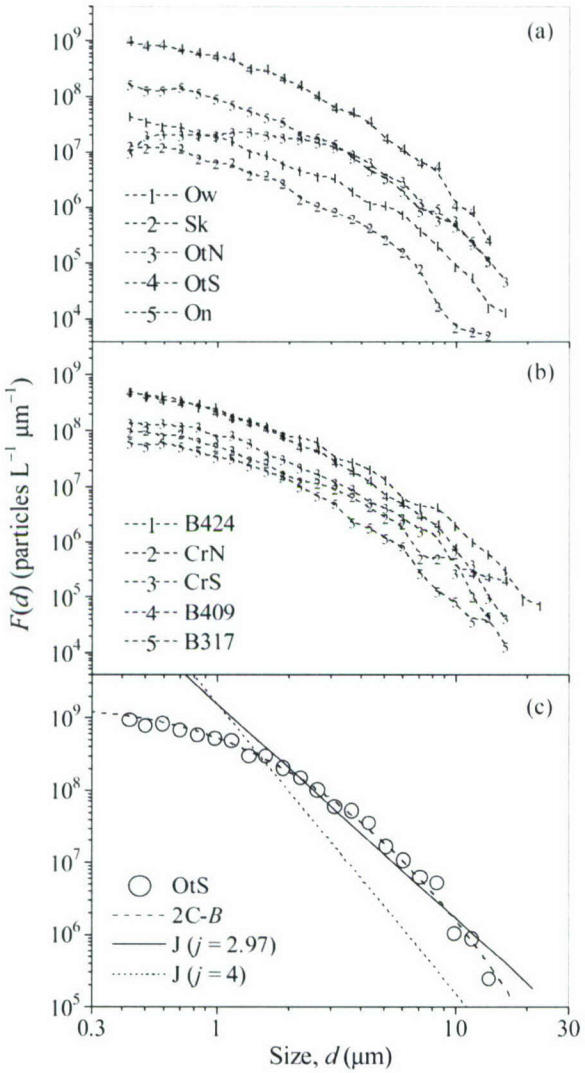

Fig. 4. PSDs for minerogenic particles: (a) five lake sites, Owasco Lake, Skaneateles Lake, north and south sites on Otisco Lake, and Onondaga Lake, (b) Seneca River system, including river buoy 424, north and south sites on Cross Lake, and river buoys 409 and 317, and (c) an example of PSD function fits [Junge (j = 2.97, with j = 4 added for reference) and 2C-*B*; OtS]. See Table 1 for site abbreviations.

D. Six Hundred Fifty Nanometers as the Reference Wavelength for *b*, Bulk Measurements of $b_p(650)$ and $b_{bp}(650)$, and Estimates of $b_m(650)$ and $b_{b,m}(650)$

The choice of λ = 650 nm as a reference wavelength (also [39]) here for b calculations does not represent a problem for comparing the results from this study with those from related studies that have adopted different wavelengths. For example, a strong (r^2 = 0.998), nearly 1:1 (slope = 1.04) linear relationship prevailed between $b_p(650)$ and the spectrally averaged (400–730 nm) scattering coefficient ($\langle b_p \rangle$; Fig. 5). Similarly strong relationships prevailed between $b_p(650)$ and other selected wavelengths, including $b_p(555)$ (Fig. 5), used by Babin *et al.* [5] as a reference wavelength. The values of $c(660)$ from the transmissometer and ac-s (separate casts) approached equivalence [$c(660)_{\text{ac-s}} = 1.09 \times c(660)_{\text{C-Star}} - 0.2$].

Table 5. 2C-*B* PSD Fitting Parameters

System[a]	C_B (l^{-1} μm^{-1})	μ_B	γ_B
OtN	5.012×10^{14}	5.25	0.288
Ow	4.21×10^{14}	1.34	0.172
Sk	1.58×10^{14}	2.64	0.226
OtS	1.29×10^{16}	2.82	0.236
On	2.12×10^{15}	2.02	0.199
B424	5.86×10^{15}	1.62	0.178
CrN	1.27×10^{15}	1.54	0.178
CrS	1.99×10^{15}	2.51	0.217
B409	5.28×10^{15}	2.06	0.202
B317	8.24×10^{14}	3.58	0.262
mean ± s.d.[b]		2.24 ± 0.72	0.208 ± 0.03

[a]See Table 1 for system abbreviations.
[b]Mean ± standard deviation, OtN not included.

Measured values of $b_p(650)$ ranged from 0.47 m^{-1} for Skaneateles Lake to 7.9 m^{-1} at B409 [Fig. 6(a)]. The value presented for the south site of Otisco Lake, the highest of the study, was estimated based on laboratory measurement of $c(660)$ (on a diluted sample) according to $b_p(650) = c(660)/1.045$ [e.g., consistent with Babin *et al.* [5] for $b_p(660)$]. Four of the sites had $b_p(650)$ values of ~4 m^{-1}, the north site of Otisco Lake, Onondaga Lake, and both the south and north sites of Cross Lake. Owasco Lake, Skaneateles Lake, and B317 had $b_p(650)$ values <2 m^{-1}.

No $b_{bp}(650)$ observation was available for the south site of Otisco Lake [Fig. 6(b)]. The pattern of differences in $b_{bp}(650)$ among the study sites was strongly correlated (r = 0.96) to that reported for $b_p(650)$. Values of $b_{bp}(650)$ ranged from 0.0034 m^{-1} for Skaneateles Lake to 0.25 m^{-1} for B424. Despite the strong correlation between $b_p(650)$ and $b_{bp}(650)$ for this population of sites, substantial differences in the backscattering ratio [$\tilde{b}_{bp}(650) = b_{bp}(650)/b_p(650)$] were observed among the sites [Fig. 6(c)]. The ratio

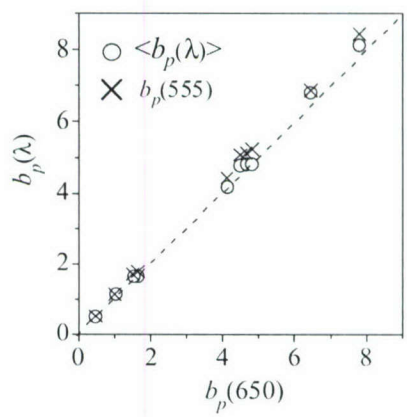

Fig. 5. Relationships between $\langle b_p(\lambda) \rangle$ and $b_p(650)$, and between $b_p(555)$ and $b_p(650)$, for study sites, with equivalence (1:1) line for reference.

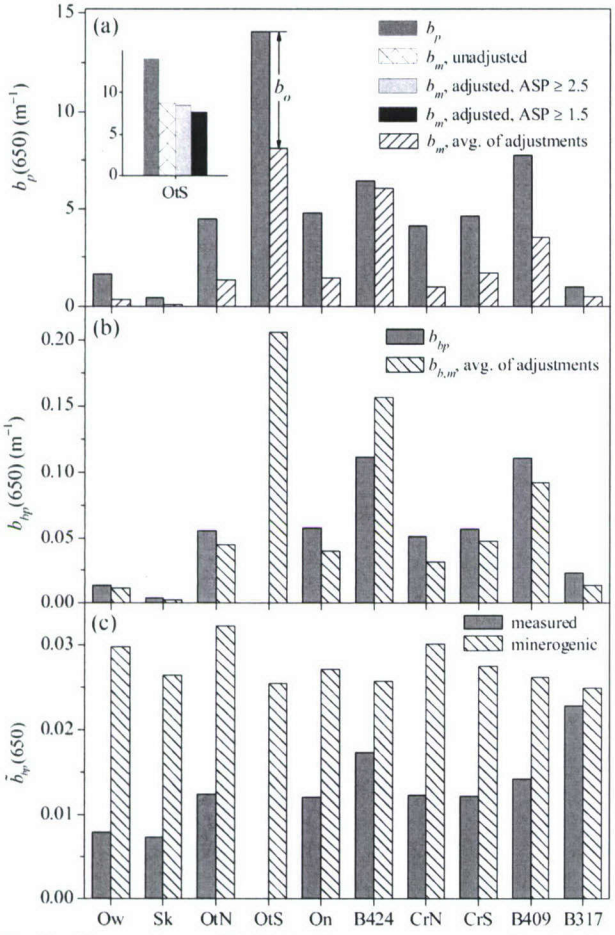

Fig. 6. Comparisons of bulk *in situ* measurements of scattering and calculated minerogenic scattering based on SAX results: (a) $b_p(650)$ and $b_m(650)$, with estimation of $b_o(650)$ illustrated, and an example of $b_m(650)$ adjusted for the lying flat effect (inset), (b) $b_{bp}(650)$ and $b_{b,m}(650)$, and (c) measured and minerogenic $\tilde{b}_{bp}(650)$. See Table 1 for site abbreviations.

was ≤0.008 for Skaneateles and Owasco Lakes, ~0.018 for B424 and ~0.023 for B317, and between 0.0125 and 0.0145 for the remaining sites.

Estimated values of $b_m(650)$, $b_{b,m}(650)$, and the corresponding minerogenic $\tilde{b}_{bp}(650)$ are presented [Figs. 6(a)–6(c)] and compared to the overall bulk measurements. Three different values were calculated for $b_m(650)$ and $b_{b,m}(650)$ for each site [one example illustrated in inset of Fig. 6(a)] that correspond to Mie theory calculations based on SAX results: (1) without adjustments for the particle "lying flat" effect, (2) with a reasonable lower bound representation of the effect (ASP ≥ 2.5), and (3) with a reasonable upper bound representation of the effect (ASP ≥ 1.5). The adjustments resulted in decreases in the estimated values of $b_m(650)$ [inset of Fig. 6(a)] and $b_{b,m}(650)$. The minimum decreases, for the lower bound adjustments, was about 4% for $b_m(650)$ and 3% for $b_{b,m}(650)$; the averages were about 5% for both features of light scattering. The maximum decreases, for the upper bound adjustments, were ~15%; the averages were 12.6 and 13.5% for $b_m(650)$ and $b_{b,m}(650)$, respectively. The single best estimate for each site is presented here [Figs. 6(a) and 6(b)] as the average of the values for upper and lower bound adjustments. These values have been used in evaluations of relationships with measurements and in estimation of $b_o(650)$ values [Fig. 6(a)].

Differences in $\langle Q_{b,m} \rangle$ (Table 6) were modest between the sites and among the minerogenic classes for individual sites (Table 6); values of $\langle Q_{b,m} \rangle$ ranged from 2.1 to 2.66 for the sites. The clay mineral values for $\langle Q_{b,m} \rangle$ were most often the lowest among the classes; the average for this class for the 10 sites was 2.23. The average for quartz (2.43), a relatively minor component of b_m, was 9% higher. The overall average $\langle Q_{bb,m} \rangle$ for the study sites was 0.061, with a coefficient of variation of 7.6%.

Comparison of calculated $b_m(650)$ and $b_{b,m}(650)$ with bulk *in situ* measurements showed that the minerogenic component was a substantial contributor to total scattering and backscattering. The minerogenic component of $b_p(650)$ ranged from ~20% at Owasco Lake to 94% at B424. This component represented from 30% to 50% of $b_p(650)$ at six of the sites; the average for all sites was 42%. These contributions

Table 6. Mean Scattering Efficiencies, $\langle Q_{b,m}(650) \rangle$,[a] of Minerogenic Particle Types for Study Sites

System	Clay	Ca-Rich Non-*Phacotus*	Quartz	Si-Rich	Ca-Agg	Miscellaneous	Total
Seneca R.							
B424	2.15	2.23	2.4	2.28	2.14	2.48	2.18
Cross L. North	2.29	2.19	2.44	2.15	2.23	2.17	2.22
Cross L. South	2.24	2.12	2.28	2.12	2.25	2.37	2.22
B409	2.19	2.43	2.4	2.14	2.27	2.32	2.23
B317	2.26	2.33	2.53	2.36	2.43	2.48	2.33
Lakes							
Owasco	2.18	2.25	2.4	2.25	2.23	2.24	2.23
Skaneateles	2.26	2.46	2.43	2.28	2.25	2.43	2.3
Otisco North	2.15	2.28	2.58	2.53	2.12	2.1	2.2
Otisco South	2.3	2.66	2.41	2.18	2.38	2.13	2.3
Onondaga	2.3	2.2	2.42	2.42	2.18	2.39	2.28

[a]For case of lying-flat adjustments for particles with ASP ≥ 1.5.

were shifted higher for backscattering. Estimates of $b_{b,m}(650)$ represented between 50% and 80% of the $b_{bp}(650)$ measurements at eight of nine sites; the average for all sites was 74%. The $b_{b,m}(650)$ estimate for B424 exceeded the $b_{bp}(650)$ observation by 30%. Estimates of the $\tilde{b}_{b,m}(650)$ varied from ~0.25 for the river sites to ~0.32 for Owasco Lake and the north site on Otisco Lake [Fig. 6(c)]. These ratio values in all cases exceeded those based on measurements, by factors of more than two, except for the river sites.

E. Relationships between Measures, Estimates, and Indicators of Scattering

TSS was a strong predictor of the differences of both $b_p(650)$ and $b_{bp}(650)$ [(Figs. 7(a) and 7(b)] among the study sites, explaining 97% ($p < 0.001$) and 94% ($p < 0.001$) of the differences, respectively, according to linear least-squares regression analysis. The mean values of $b_p(650)$/TSS and $b_{bp}(650)$/TSS ratios were 0.86 and 0.012 $m^2\ g^{-1}$, respectively. PAV_m was a strong predictor of the observed differences in $b_p(650)$ and $b_{bp}(650)$ [(Figs. 7(c) and 7(d)], explaining 96% ($p < 0.001$) of the differences in both cases, a result consistent with the performance of FSS_{corr} in predicting $c(660)$ [Eq. (9)].

FSS_{corr} was nearly as strong a predictor of the estimated values of $b_m(650)$ and $b_{b,m}(650)$ [Figs. 7(e) and 7(f)] as TSS was for the overall bulk scattering metrics, accounting for 95% ($p < 0.001$) of the variations in both estimates. The mean values of the $b_m(650)/FSS_{corr}$ and $b_{b,m}(650)/FSS_{corr}$ ratios were 0.62 and 0.017 $m^2\ g^{-1}$, respectively. Significant relation-

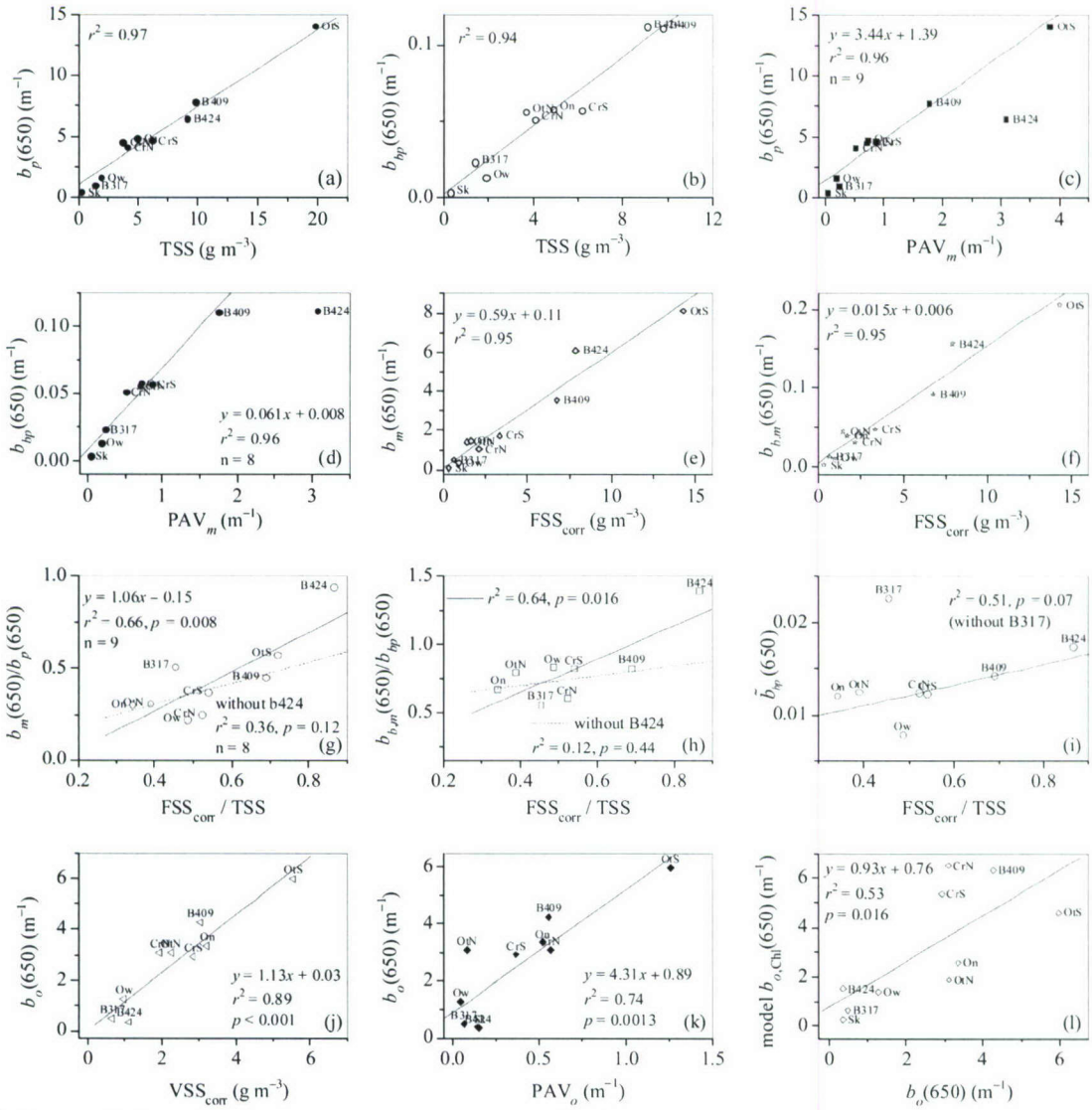

Fig. 7. Evaluation of relationships between measures, estimates, and indicators of scattering for the study sites: (a) $b_p(650)$ versus TSS, (b) $b_{bp}(650)$ versus TSS, (c) $b_p(650)$ versus PAV_m (B424 as outlier in regression analysis), (d) $b_{bp}(650)$ versus PAV_m (B424 as outlier in regression analysis), (e) $b_m(650)$ versus FSS_{corr}, (f) $b_{b,m}(650)$ versus FSS_{corr}, (g) $b_m(650)/b_p(650)$ versus FSS_{corr}/TSS, (h) $b_{b,m}(650)/b_{bp}(650)$ versus FSS_{corr}/TSS, (i) $\tilde{b}_{bp}(650)$ versus FSS_{corr}/TSS, (j) $b_o(650)$ versus VSS_{corr}, (k) $b_o(650)$ versus PAV_o, and (l) $b_o(650)$ versus $b_{o,Chl}(650)$. See Table 1 for site abbreviations.

ships were observed between the FSS_{corr}/TSS ratio and the $b_m(650)/b_p(650)$ ratio [Fig. 7(g)] as well as the $b_{b,m}(650)/b_{bp}(650)$ ratio [Fig. 7(h)]. However, the observations for B424 had a disproportionate effect in both cases; the relationships were not significant if the values for that site were omitted, and in the case of $b_{b,m}$, the estimate exceeded the measured [Fig. 7(h)]. Some positive dependence between $\tilde{b}_{bp}(650)$ and FSS_{corr}/TSS was observed across the study sites [Fig. 7(i)]; however, even with B317 as an outlier, the relationship was not significant at $\alpha = 0.05$ ($p = 0.07$).

A strong linear relationship ($r^2 = 0.89$, $p < 0.001$), with a relatively small y intercept, prevailed between $b_o(650)$ [$=b_p(650) - b_m(650)$] and VSS_{corr} across the study sites [Fig. 7(j)]. The mean $b_o(650)/VSS_{corr}$ ratio was 1.08 $m^2\ g^{-1}$ for the study sites. The relationship observed between $b_o(650)$ and the PAV associated with organic particles [PAV_o, Fig. 7(k); estimated as the sum of *Phacotus* and the Organics and Diatoms classes, without lying flat adjustments] was nearly as strong. The best fit relationship between calculated $b_o(650)$ and the independently estimated $b_{o,Chl}(650)$ approached 1:1, though it was less strong ($r^2 = 0.53$, $p = 0.02$) [Fig. 7(l)].

F. Size Dependencies of Scattering and Sensitivity to n Value

Calculated (Mie theory) cumulative size distributions of $b_m(650)$ and $b_{b,m}(650)$, based on SAX observations, are presented to depict the contributions of various particle sizes for a Seneca River (B424) site [Figs. 8(a) and 8(b)]. These patterns are generally representative of those obtained for all the study sites. Particles within the size range 2–10 μm contributed the most to both $b_m(650)$ and $b_{b,m}(650)$. Larger particles were generally unimportant due to their scarceness, as depicted by the "leveling off" of plots for $d > \sim 10$ μm. Submicron particles made <2% contributions to scattering. The size contribution patterns were generally similar for $b_m(650)$ and $b_{b,m}(650)$. The size that corresponds to 50% of the total value (i.e., particles less than or equal to that size are responsible for 50% of the scattering; d_{50}) is a useful attribute of the patterns. The d_{50} values for both $b_m(650)$ and $b_{b,m}(650)$ for the river site were ~5.2 μm.

The size dependency patterns of scattering were also simulated with uniform m ($1.17-0.005i$) for three cases of PSDs: observed, best fit Junge, and Junge with $j = 4$ (curves in Fig. 8), and the simulations for the Junge cases were extended down to a size of 0.1 μm. The simulation performed for the measured PSDs (with uniform m) tracked the observed patterns closely. Consistent with the shortcomings of the best fit Junge function in fitting the observed PSDs [e.g., Fig. 4(c)], this function overrepresented the scattering effects of submicrometer particles and predicted continuing strong increases in scattering for $d > 10$ μm, and generally deviated from observations for intermediate sizes (Fig. 8). The deviations of the shapes of the patterns for $j = 4$ were even greater

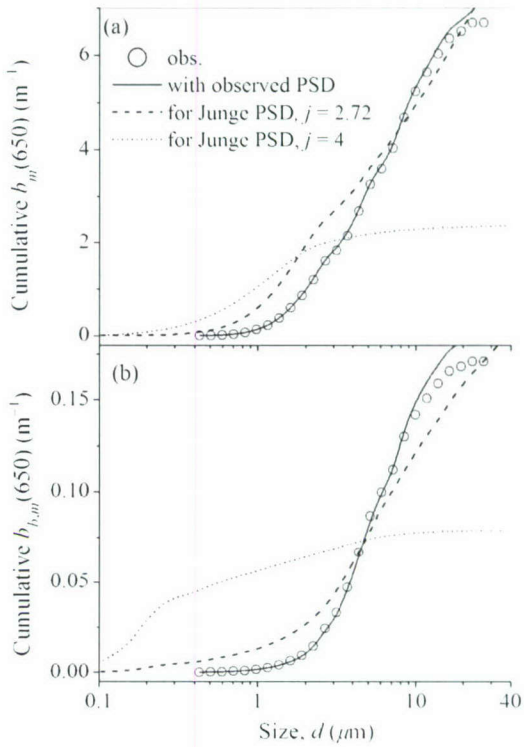

Fig. 8. Size dependencies of scattering coefficients as cumulative plots, based on observations (symbols) from Seneca River at buoy 424, and simulations from three cases of PSDs (observed, and Junge with best fitted j and invoked $j = 4$; curves) with uniform $m = 1.17-0.0005i$: (a) $b_m(650)$, and (b) $b_{b,m}(650)$.

(for the case of maintaining the same C value; Fig. 8). In contrast, the 2C-B fits supported cumulative scattering patterns (not shown) that tracked those based on observations closely, consistent with their good fits of the observed PSDs in the size range that was important to scattering.

Contrasting patterns emerged for the dependencies of $b_m(650)$ and $b_{b,m}(650)$ on n, as illustrated for the Owasco Lake sample [Figs. 9(a) and 9(b)]. Values are presented relative to the predictions for $n = 1.25$ to support comparisons for the observed PSDs and Junge function representations. The predicted patterns for this site were qualitatively representative of the others included in this study. Values of $b_m(650)$ were predicted to be relatively invariant over the evaluated range of n (1.05–1.25) for the observed PSDs [Fig. 9(a)], whereas progressive increases in $b_{b,m}(650)$ were predicted throughout the range for the observed PSDs [Fig. 9(b)]. Junge function scenarios for the PSDs deviated from the observed, demonstrating a greater positive dependence on n, with an even stronger effect for $j = 4$ compared to the best fit value of 2.68.

4. Discussion

A. Importance and Partitioning of the Minerogenic Particle Assemblage

The central role minerogenic particles played in regulating differences in light-scattering levels between

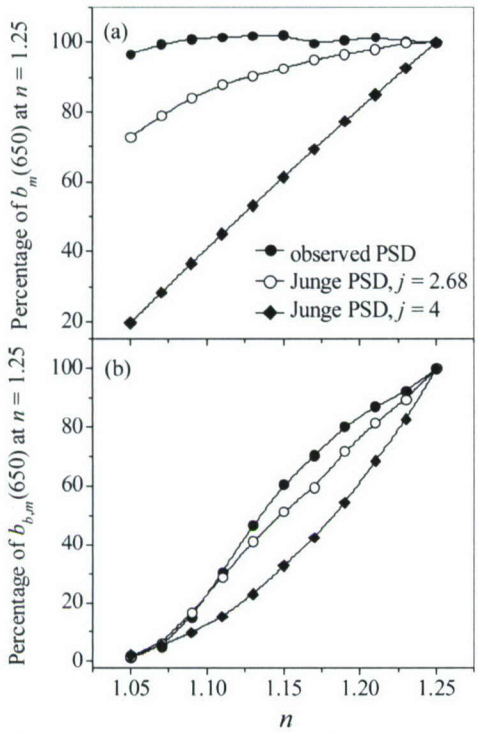

Fig. 9. Scattering as functions of n (with $n' = 0.0005$), for observed minerogenic PSD at Owasco Lake, for Junge PSDs with fitted j values of 2.68 and commonly invoked 4: (a) $b_m(650)$ as percentages of the values calculated for $n = 1.25$ (0.41, 0.45, and 0.22 m^{-1} for the three cases of PSDs, respectively), and (b) $b_{b,m}(650)$ as percentages of the values calculated for $n = 1.25$ (0.016, 0.016, and 0.0092 m^{-1} for the three cases of PSDs, respectively).

the study systems was manifested in empirical analyses with common metrics of water quality [Eq. (9)], as well as by the dependence of both $b_p(650)$ and $b_{bp}(650)$ on PAV_m [Figs. 7(c) and 7(d)]. Increasingly, lakes and reservoirs have been identified where minerogenic particles are important in regulating scattering and apparent optical properties (AOPs). For example, Peng and Effler [27] reported that PAV_m was a stronger ($r^2 = 0.82$) predictor than Ch1 ($r^2 = 0.56$) of Secchi depth differences between the eleven Finger Lakes of New York (see also[29,40,41]). Moreover, distinct temporal structure in optical characteristics in freshwater systems can be imparted by dynamics in terrigenous inputs [15] and autochthonous precipitation of minerogenic particles [29,42]. The origin of optically important particles (allochthonous versus autochthonous) is essential information for managers concerned with identifying appropriate targets and rehabilitation approaches for improved optical esthetics, and for proper interpretation of bulk optical measurements.

Despite the inherent limitations of a single sampling, the PAV_m results are generally consistent with known characteristics of the study systems. All of the study lakes are known to be oversaturated with respect to calcite, and to experience precipitation of $CaCO_3$ in the upper waters during summer [29,42,43]. The spatial PAV patterns for clay mineral particles and diatoms from upstream, within, and just downstream of Cross Lake reflect the incomplete mixing of the river inflow within this lake [16] and the functioning of the lake as a source of phytoplankton [e.g., diatoms; see also Fig. 2(c)] to downstream portions of the river [17]. The decrease in PAV_m (Table 3) and FSS_{corr} [Fig. 2(b)] between B409 and B317 reflects the effects of the nonselective filter feeding by zebra mussels [44]; this sink for inorganic (as well as organic) particles has contributed importantly to the increased clarity observed over this reach since the invasion [45] by this exotic bivalve.

This paper has embraced the reductionist approach described by Stramski and co-workers [7,8] by partitioning the minerogenic fraction of scattering into multiple components. SAX could support partitioning of the minerogenic assemblage into more particle classes than the number adopted here. For example, Yin and Johnson [46] used a particle classification scheme that delineated 18 minerogenic classes, including five types of clay minerals, in applying SAX for a particle-class budget analysis of Onondaga Lake sediments. Such schemes use tighter boundaries for the elemental stoichiometries of the particle classes, and implicitly are accompanied by greater uncertainty with regards to the proper classification of individual particles. While such an approach may be appropriate for specific issue/ecosystem combinations, the simpler scheme adopted here (Table 2) served to resolve the fundamentally different origins of the important components of the minerogenic particle assemblages of these study systems. Further compression of the terrigenous particle types into fewer classes is not desirable, even though the n values are similar, as differences in n' may have important implications with respect to remote-sensing reflectance spectral signatures [35].

B. Implementation of the Forward Method, Partitioning $b(\lambda)$

Advancement of the reductionist approach to partition scattering requires implementation of the forward method, the calculation of scattering attributable to noteworthy particle classes based on particle information. Limitations in our implementation of the forward method have two sources: (1) uncertainties in the information supplied to the calculation framework, and (2) application of the Mie theory for the documented particle populations. The capability of SAX to characterize individual minerogenic particles both compositionally and morphometrically supports the advancement of the forward method. There are modest imperfections in both regards relative to supporting forward calculations. For example, there are only minor uncertainties in the partitioning of minerogenic particles for the simple classification strategy adopted because of the conspicuous elemental differences (Table 2). Given the elemental composition information from SAX, the greater uncertainty lies in the specification of n values based on the literature. Noteworthy variations in n are associated with the various clay minerals and the source of the value for

$CaCO_3$ (calcite) (1.24 by Twardowski *et al.* [47] and 1.173 by Woźniak and Stramski [35]). Estimates of $b_m(650)$ were insensitive to minerogenic n values for the PSDs encountered at the study sites [Fig. 9(a)]. However, estimates of $b_{b,m}(650)$ were sensitive to this source of uncertainty [Fig. 9(b)], indicating the importance of the composition information from SAX in guiding specification of n in calculations of backscattering. SAX provides a robust representation of particle PA. The shortcoming of lying flat on the filter in SAX is modest compared to that associated with Coulter counter data for irregularly shaped particles. Such counters infer particle sizes from measured electrical resistance of particles based on their volumes, leading to systematic underestimation of particle sizes (calculated from volume equivalent spheres) for nonspherical particles. The presented bounds for the lying flat effect are believed to reasonably bracket the effect.

The Mie theory stipulations of particle sphericity and homogeneity were not met for the minerogenic particles of this study, as reflected by the ASP values (Table 4) and substantial concentrations of aggregates of minerogenic classes (e.g., Ca-agg; Table 3). These deviations need to be considered in context. First, the heterogeneity associated with partial coating of particles with $CaCO_3$ is a minor effect given the similarity of n values for the various classes (Table 2) and the insensitivity of $b_m(650)$ estimates to variations in n (Fig. 9). Second, it has long been recognized that most oceanic (and presumably freshwater) particles are not spherical [14]. Deviations from sphericity can cause substantial shifts in $\beta_p(\theta)$, though these effects influence light scattered in the backward direction more than in the forward (and primary) direction [6,48,49]. Both positive and negative effects of deviations from sphericity on $b_{bp}(\lambda)$ have been reported [50,51]. The effect of particle shape for randomly oriented particles on $\langle Q_b \rangle$ (and consequently b_p) is apparently small by comparison [14,48,52]. Thus we have relatively more confidence in our Mie theory estimates of $b_m(650)$ than those of $b_{b,m}(650)$. Mie theory calculations represent the only viable, albeit imperfect, vehicle to estimate both $b_m(\lambda)$ and $b_{b,m}(\lambda)$ based on individual particle information for thousands of particles that differ in size and composition [53]. More complex modeling, if feasible for such heterogeneous particle populations, would still be accompanied by substantial uncertainty that is difficult to assess [53]. Minerogenic particles such as those encountered in our study (e.g., Fig. 3) represent less complex problems in light scattering compared to many microorganisms with respect to geometry [51] and the potential for layered effects within microorganisms [8], though variation in the degree of hydration [20] may be an issue (albeit modest) for clay minerals.

Despite the deviations of the particle populations from the simplifying assumptions of Mie theory, the evidence is strong that SAX can support the partitioning of the minerogenic component of scattering in these fresh waters according to the relative contributions of important particle classes. This partitioning can reasonably be based directly on PAV_m results delineated according to designated classes (Table 3). This position is supported by the general similarities of $\langle Q_{b,m} \rangle$ (Table 6; embedded effects of m and PSD) and ASP representations of shape for the various classes (Table 4). Accordingly, percent contributions of the various minerogenic particle classes to PAV_m correspond to contributions to b_m; e.g., clay minerals represented ~70% of $b_m(650)$ at the upstream river site (B424) and calcite (non-*Phacotus* Ca-rich) was responsible for ~35% of $b_m(650)$ in Owasco Lake (Table 3).

Demonstration of closure of the SAX-based estimates with independent measures of minerogenic scattering is difficult for natural waters because particle populations are composed of mixtures of minerogenic and organic particles. The closure between SAX-based estimates of $b_m(660)$ and measurements of $c(660)$ demonstrated for Schoharie Reservoir, where clay particles dominate scattering [15], is supportive of the minerogenic scattering estimates presented here. None of the sites of this study demonstrated the extent of dominance by minerogenic particles [e.g., Fig. 2(b)] reported for Schoharie Reservoir. However, the significant, nearly 1:1 relationship between the calculated $b_o(650)$ values and independent estimates of $b_{o,Chl}(650)$ suggests a degree of closure. Much of the observed scatter in the relationship may reflect the limitations of Chl as a surrogate metric of the overall organic particle population. Moreover, the array of measured and estimated conditions included in this study offered multiple tests of consistency that generally support the SAX-based estimates of minerogenic scattering. This is supported by the strong relationships between the gravimetric measure of minerogenic suspended solids (FSS_{corr}) and $b_m(650)$ [Fig. 7(e)], and between FSS_{corr} and $b_{b,m}(650)$ [Fig. 7(f)]. Further, the ratios of $b_m(650)$ to $b_p(650)$, and $\tilde{b}_{bp}(650)$, were positively related to the FSS_{corr}/TSS [Figs. 7(g) and 7(i)]. Additional support for the $b_m(650)$ predictions is provided by the consistency of the $b_o(650)$ estimates with indicators of the organic particle population, including the strong relationships between $b_o(650)$ and VSS_{corr} [Fig. 7(j)], and between $b_o(650)$ and PAV_o [Fig. 7(k)]. Overall, the empirical indicators of the performance of SAX in supporting the partitioning of $b_p(\lambda)$ into $b_m(\lambda)$ and $b_o(\lambda)$ are promising. We have not pursued similar partitioning for $b_{bp}(\lambda)$ here because of the greater uncertainty associated both with the Mie estimates of $b_{b,m}(\lambda)$ and empirical relationships to predict $b_{b,o}(\lambda)$ based on Chl [38].

The extent of consistency of the scattering estimates depends importantly on the representativeness of the samples relative to the field instrumentation measurements. The general consistency of the $b_p(650)/TTS$ ratios observed here with the marine literature [5] offers only coarse support for the representativeness of the samples. Space-time differences in the waters sampled and analyzed in the laboratory ver-

sus measured *in situ*, associated with patchy distributions of particles (e.g., Babin *et al.* [5]), likely contributed to the observed scatter in the relationships (Fig. 7) and the inconsistent case of $b_{b,m}(650) > b_{bp}(650)$ at B424 [Fig. 6(b)]. The modest variations in the relationship between the ac-s and C-Star measurements of $c(660)$ among the sites suggests that such monitoring limitations likely contributed to imperfect relationships.

C. Minerogenic Particle Size Distributions

Presentation of detailed minerogenic PSDs that included submicrometer particles (e.g., Fig. 4) has been rare. Lambert *et al.* [54] used scanning electron microscopy integrated with an electron microprobe technique to characterize the PSDs of minerogenic particles ≥ 0.2 μm in 15 samples from seven ocean sites. They reported a leveling-off of particle concentrations for sizes <0.7 μm, deviating strongly from a Junge function, and represented the PSDs by lognormal distributions instead. The PSDs reported here (Fig. 4) had similar patterns to those reported recently [15] for Schoharie Reservoir, based on SAX measurements; e.g., conspicuous decreases in $F(d)$ for sizes smaller than the frequency peak size (exception for north site of Otisco Lake) within the submicrometer range. We are unaware of any direct measurements that included submicrometer observations for either marine or fresh waters to support the Junge function as representative of minerogenic PSDs. Coulter counters cannot address this issue because the lower size threshold is too high, and these instruments fail to differentiate minerogenic from organic particles.

Characterization of PSDs has received extensive attention for marine systems [2,55]. A number of functional representations of PSDs have been used, including the hyperbolic (or Junge) model, the lognormal distribution [54], segmented lognormal functions [2], the TCM, and segmented hyperbolic distributions [55]. The Junge function was supported in earlier studies that used electronic particle counters (e.g., [56]), and has been widely adopted in modeling [1,5,7] and inversion analyses [47,57]. An exception was the inclusion of the TCM, in addition to a Junge function, in a modeling analysis by Twardowski *et al.* [47]. Further evaluation is needed to test the applicability of 2C-*B* as well as other functions in representing PSDs in other fresh waters. Other models may also fit the observations, particularly the lognormal function. The generality of such models is important to support inversion algorithms.

Babin *et al.* [5] predicted submicrometer mineral particles ($n = 1.18$) contribute substantially to b_m in marine waters, with a value of $d_{50} \sim 1$ μm for $j = 4$ based on Mie theory calculations (our simulations of the size dependency patterns of scattering adopting $j = 4$ resulted in a similar conclusion; dotted curves in Fig. 8). Accordingly, those investigators suggested that the determination of the b_p/SPM ratio may be sensitive to the porosity of the filter used in their SPM analyses (glass fiber GF/F filters, 0.7 μm pore size). Our observations for these freshwater systems are strikingly different in that regard. Submicrometer minerogenic particles did not make noteworthy contributions to scattering according to Mie theory calculations based on SAX data (Fig. 8); e.g., $d_{50} \sim 4$ μm. Moreover, the effective pore size(s) of glass fiber filters have been reported to be less than the nominal sizes [58,59] (e.g., effective size of our filters <1.5 μm; a better choice would have been GF/F with a nominal pore size of 0.7 μm). Under these conditions, the effective pore size of the filters used in the TSS analyses does not represent a noteworthy source of uncertainty for the $b_m(650)/\mathrm{FSS}_{\mathrm{corr}}$ ratio. We cannot eliminate the possibility that large quantities of submicrometer organic particles were present and passed through the filters and thereby caused the $b_o(650)/\mathrm{VSS}_{\mathrm{corr}}$ and $b_p(650)/\mathrm{TSS}$ ratios to be false high. However, review of the available particle size information for the Organics class for the study sites suggests submicron organic particles were not important.

The limitations in the best fit J function in matching the observed PSDs of this study resulted in noteworthy systematic shortcomings in representation of the dependence of $b_m(650)$ and $b_{b,m}(650)$ on particle size (Fig. 8). For example, though the predicted $b_m(650)$ approximately matched that based on observations through a size range extending to ~20 μm, the size trajectory of the relationships deviated substantially, and unrealistic strong increases beyond the sizes of SAX observations (i.e., >20 μm) were predicted [Fig. 8(a)]. Similar shortcomings of the J function in representing the size dependence of b_m have been reported by Stavn and Keen [60]. Moreover, invoking a J functional representation of the minerogenic PSDs of this study caused the dependence of calculations of $b_m(650)$ and $b_{b,m}(650)$ on n (i.e., particle composition) to be overstated (Fig. 9).

D. Backscattering

Great uncertainty persists concerning the origins of backscattering in both marine [8,38,39] and freshwater [9] systems, a key issue in remote sensing [50]. Stramski *et al.* [8] described the dominant fraction of backscattering that was not accounted for by microorganisms as the "missing backscattering enigma." Submicrometer nonliving (particularly inorganic) particles were identified as the likely responsible component in the open ocean under nonbloom conditions because these particle sizes make relatively greater contributions to $b_{bp}(\lambda)$ than to $b_p(\lambda)$ [1,7]. Similarly, modeling analyses by Woźniak and Stramski [35] depicted the potential importance of submicrometer minerogenic particles in influencing ocean reflectance. Modeling analyses by Stramski *et al.* [7], based on speculative concentrations and PSDs ($j = 4$), suggested that submicrometer minerogenic particles were important for $b_p(\lambda)$ and dominated $b_{bp}(\lambda)$ in ocean waters. The argument that backscattering is largely regulated by submicrometer particles has been influenced greatly by the lack of direct measurements of these colloidal particles, which has necessitated extrapolation of fitted or assumed functions

into this size range. Risović [4] demonstrated that $\tilde{b}_{bp}(\lambda)$ depended strongly on the trajectory of the extrapolation and thus the specified relationship to describe the PSD. Based on comparative fits of the Junge and the TCM to observed ocean PSDs ($d > 0.8$ μm), Risović [4] demonstrated that application of the Junge function resulted in substantial overprediction of the $\tilde{b}_{bp}(\lambda)$, as a result of overestimation of concentrations of submicrometer particles.

Several features of the results established that submicrometer minerogenic particles were not important contributors to $b_{bp}(650)$: (1) the observed PSDs were fitted well with the 2C-*B* function, (2) the magnitude of $b_{b,m}(650)$ relative to the $b_{bp}(650)$ observations [Fig. 6(b)], (3) the size trajectories of $b_{b,m}(650)$ [Figs. 8(b) and 8(d)], and (4) the lack of dependence of ASP on d. The case of invoking $j = 4$ for the PSDs of this study demonstrates the preferential effect on $b_{b,m}(650)$ versus $b_m(650)$ for dependencies on d (Fig. 8). Accordingly, ~60% of the total $b_{b,m}(650)$ would be associated with submicrometer particles, compared to ~45% for total $b_m(650)$. Given the strong dependency of b_{bp} on composition [e.g., Fig. 9(b)], SAX offers opportunities to advance future efforts to demonstrate closure in forward method for estimates of b_m and $b_{b,m}$ with bulk measurements, particularly for systems enriched with minerogenic particles.

The particulate backscattering ratio ($\tilde{b}_{bp}$) is concentration independent, and relevant to remote sensing, light field modeling, and inference of bulk refractive index from optical measurements [39,61]. Whitmire *et al.* [61] presented 20% as a conservative estimate of the likely maximal error of $\tilde{b}_{bp}$ based on a propagation of error analysis for similar field instrumentation measurements of bulk conditions (absorption and attenuation meter over nine wavelengths, ac-9, HydroScat). The ratio value is sensitive to composition (generally higher where inorganic particles make greater relative contributions) and PSDs [39,61]. While the data set presented here is modest in size [Fig. 6(c)] compared to recently published compilations from extensive marine surveys of the ratio [39,61], this study of freshwater systems has the advantage of more definitive specification of the minerogenic component of b_{bp}. The estimates of the ratio for the minerogenic particles [$\tilde{b}_{b,m}$; Fig. 6(c)] represent upper bound values of $\tilde{b}_{bp}$ corresponding to the scenario of no organic (e.g., phytoplankton) particles. The modest differences in the $\tilde{b}_{b,m}$ values among sites [Fig. 6(c)] reflect differences in PSDs and composition of minerogenic particles. The observed $\tilde{b}_{bp}(650)$ values from bulk measurements can be viewed as the outcome of the mixture of $\tilde{b}_{b,m}(650)$ values with the lower values associated with low n organic particles. The differences in the $\tilde{b}_{bp}$ values were generally consistent with the simple view of the mixing of different relative amounts of minerogenic and organic particles, as indicated by the dependency of $\tilde{b}_{bp}$ on the FSS_{corr}/TSS ratio [Fig. 7(i)]. Loisel *et al.* [39] also reported lower $\tilde{b}_{bp}$ values for particle populations dominated by (organic) material of low refractive indexes and high values for sites with relatively high concentrations of inorganic particles. The population of $\tilde{b}_{bp}(650)$ values from this study was consistent with those reported in the marine compilations [39,61] from widely different scattering conditions (contributions of inorganic versus organic particles). For example, our mean $\tilde{b}_{bp}$ value was 0.0132 compared to 0.0138 reported by Loisel *et al.* [39], and a geometric mean of 0.013 reported by Whitmire *et al.* [61]. Moreover, our higher values were within the upper 20% of $\tilde{b}_{bp}$ populations in the marine surveys where the elevated backscattering ratios were attributed to enrichment with mineral particles.

E. Advancing the Forward Method for Light Scattering

Various initiatives would improve the credibility of estimates of the minerogenic component of light scattering based on SAX data, and support the approach to optical closure. Paired measurements of $\beta_p(\theta, \lambda)$ [62] would more rigorously define $b_p(\lambda)$ and particularly $b_{bp}(\lambda)$, and the limitations of Mie theory estimates. Such information would be especially valuable for cases where minerogenic particles are dominant. The combination of well-defined particle morphometry from SAX and detailed $\beta_p(\theta, \lambda)$ information could guide the development of empirical adjustment approaches, or application of more complex formulations of light scattering [50], for cases where application of Mie theory to estimate scattering is inappropriate or found to be flawed. Improved quantification of PAV_o, and thereby $b_o(\lambda)$, through modification of SAX techniques would improve closure for overall $b_p(\lambda)$. For example, heavy metal staining has been used to improve detection and resolution of organic particle features with SAX [63]. Peng and Effler [15] have described approaches to reduce the modest uncertainty associated with the lying flat effect on SAX analyses.

To assess the applicability of the findings reported here, minerogenic PSDs that extend into the submicron range should be documented with SAX, and Mie theory estimates should be made, in concert with bulk scattering measurements, for a wide range of freshwater and marine systems. Investigations focusing on conspicuous light-scattering signatures imparted by minerogenic particles from runoff (clay minerals) or "whiting" ($CaCO_3$ precipitation) events represent opportunities to advance testing of the approaches presented here.

This study was funded by the Naval Research Laboratory. Sampling and field measurements were conducted by B. Wagner, M. Spada, A. Prestigiacomo, N. Osborne, and J. Denkenberger. Gina Quaring and Jennifer Aicher performed laboratory analyses of turbidity and chlorophyll concentrations, respectively. We thank Minsu Kim for his help in explaining the BHMie algorithm for backscattering calculations. We appreciate the constructive comments by anonymous

reviewers. This is contribution 251 of the Upstate Freshwater Institute.

References

1. D. Stramski and D. A. Kiefer, "Light scattering by microorganisms in the open ocean," Prog. Oceanogr. **28,** 343–383 (1991).
2. M. Jonasz and G. Fournier, "Approximation of the size distribution of marine particles by a sum of log-normal functions," Limnol. Oceanogr. **41,** 744–754 (1996).
3. E. Boss, W. S. Pegau, W. D. Gardner, J. R. V. Zaneveld, A. H. Barnard, M. S. Twardowski, G. C. Chang, and T. D. Dickey, "Spectral particulate attenuation and particle size distribution in the bottom boundary layer of a continental shelf," J. Geophys. Res., [Oceans] **106,** 9509–9516 (2001).
4. D. Risović, "Effect of suspended particulate-size distribution on the backscattering ratio in the remote sensing of seawater," Appl. Opt. **41,** 7092–7101 (2002).
5. M. Babin, A. Morel, V. Fournier-Sicre, F. Fell, and D. Stramski, "Light scattering properties of marine particles in coastal and open ocean waters as related to the particle mass concentration," Limnol. Oceanogr. **48,** 843–859 (2003).
6. M. I. Mishchenko and L. D. Travis, "Light scattering by polydispersions of randomly oriented spheroids with sizes comparable to wavelengths of observation," Appl. Opt. **33,** 7206–7225 (1994).
7. D. Stramski, A. Bricaud, and A. Morel, "Modeling the inherent optical properties of the ocean based on the detailed composition of the planktonic community," Appl. Opt. **40,** 2929–2945 (2001).
8. D. Stramski, E. Boss, D. Bogucki, and K. J. Voss, "The role of seawater constituents in light backscattering in the ocean," Prog. Oceanogr. **61,** 27–56 (2004).
9. R. P. Bukata, J. H. Jerome, K. Y. Kondratyev, and D. V. Pozdnyakov, *Optical Properties and Remote Sensing of Inland and Coastal Waters* (CRC, 1995).
10. J. T. O. Kirk, *Light and Photosynthesis in Aquatic Ecosystems* (Cambridge U. Press, 1994).
11. C. D. Mobley, *Light and Water: Radiative Transfer in Natural Waters* (Academic, 1994).
12. S. W. Effler and M. G. Perkins, "An optics model for Onondaga Lake," Lake Reserv. Manage. **12,** 115–125 (1996).
13. S. W. Effler, *Limnological and Engineering Analysis of a Polluted Urban Lake: Prelude to Environmental Management of Onondaga Lake, New York* (Springer, 1996).
14. M. Jonasz, "Nonsphericity of suspended marine particles and its influence on light scattering," Limnol. Oceanogr. **32,** 1059–1065 (1987).
15. F. Peng and S. W. Effler, "Suspended minerogenic particles in a reservoir: light-scattering features from individual particle analysis," Limnol. Oceanogr. **52,** 204–216 (2007).
16. S. W. Effler and C. F. Carter, "Spatial variability in selected physical characteristics and processes in Cross Lake, New York," Water Resour. Bull. **23,** 243–250 (1987).
17. S. W. Effler, D. A. Matthews, C. M. Brooks–Matthews, M. Perkins, C. A. Siegfried, and J. M. Hassett, "Water quality impacts and indicators of metabolic activity of the zebra mussel invasion of the Seneca River," J. Am. Water Resour. Assoc. **40,** 737–754 (2004).
18. L. S. Clesceri, A. E. Greenberg, and A. D. Eaton, eds., *Standard Methods for the Examination of Water and Wastewater* (American Public Health Association, American Water Works Association, Water Environment Federation, 1998).
19. T. R. Parsons, Y. Maita, and C. M. Lalli, *A Manual of Chemical and Biological Methods for Seawater Analysis* (Pergamon, 1984).
20. A.-L. Barillé–Boyer, L. Barille, H. Masse, D. Razet, and M. Heral, "Correction for particulate organic matter as estimated by loss on ignition in estuarine ecosystems," Estuarine Coastal Shelf Sci. **58,** 147–153 (2003).
21. WET Labs, "Spectral absorption and attenuation meter ac-s: user's guide" (Philomath, Oregon, USA, 2006).
22. W. S. Pegau, D. Gray, and J. R. V. Zaneveld, "Absorption and attenuation of visible and near-infrared light in water: dependence on temperature and salinity," Appl. Opt. **36,** 6035–6046 (1997).
23. J. Piskozub, D. Stramski, E. Terrill, and W. K. Melville, "Influence of forward and multiple light scatter on the measurement of beam attenuation in highly scattering marine environments," Appl. Opt. **43,** 4723–4731 (2004).
24. WET Labs, "Scattering meter BB9: user's guide" (Philomath, Oregon, USA, 2007).
25. E. Boss and W. S. Pegau, "Relationship of light scattering at an angle in the backward direction to the backscattering coefficient," Appl. Opt. **40,** 5503–5507 (2001).
26. F. Peng, D. L. Johnson, and S. W. Effler, "Suspensoids in New York city's drinking water reservoirs: Turbidity apportionment," J. Am. Water Resour. Assoc. **38,** 1453–1465 (2002).
27. F. Peng and S. W. Effler, "Inorganic tripton in the Finger Lakes of New York: importance to optical characteristics," Hydrobiologia **543,** 259–277 (2005).
28. D. L. Johnson, J. Jiao, S. G. DosSantos, and S. W. Effler, "Individual particle analysis of suspended materials in Onondaga Lake, New York," Environ. Sci. Technol. **25,** 736–744 (1991).
29. A. D. Weidemann, T. T. Bannister, S. W. Effler, and D. L. Johnson, "Particulate and optical properties during $CaCO_3$ precipitation in Otisco Lake," Limnol. Oceanogr. **30,** 1078–1083 (1985).
30. J. C. Russ, *The Image Processing Handbook* (CRC, 1998).
31. Y. C. Agrawal and H. C. Pottsmith, "Instruments for particle size and settling velocity observations in sediment transport," Mar. Geol. **168,** 89–114 (2000).
32. D. Risović, "Two-component model of sea particle size distribution," Deep-Sea Res., Part I **40,** 1459–1473, doi:doi: 10.1016/0967-0637(93)90123-K (1993).
33. C. F. Bohren and D. R. Huffman, *Absorption and Scattering of Light by Small Particles* (Wiley, 1983).
34. P. F. Kerr and A. F. Rogers, *Optical Mineralogy* (McGraw-Hill, 1977).
35. S. B. Woźniak and D. Stramski, "Modeling the optical properties of mineral particles suspended in seawater and their influence on ocean reflectance and chlorophyll estimation from remote sensing algorithms," Appl. Opt. **43,** 3489–3503 (2004).
36. T. D. Proctor and G. W. Harris, "The turbidity of suspensions of irregular quartz particles," J. Aerosol Sci. **5,** 81–90 (1974).
37. H. Loisel and A. Morel, "Light scattering and chlorophyll concentration in case 1 waters: a reexamination," Limnol. Oceanogr. **43,** 847–858 (1998).
38. A. Morel and S. Maritorena, "Bio-optical properties of oceanic waters: a reappraisal," J. Geophys. Res., [Oceans] **106,** 7163–7180 (2001).
39. H. Loisel, X. Mériaux, J.-F. Berthon, and A. Poteau, "Investigation of the optical backscattering to scattering ratio of marine particles in relation to their biogeochemical composition in the eastern English Channel and southern North Sea," Limnol. Oceanogr. **52,** 739–752 (2007).
40. S. W. Effler, D. A. Matthews, M. Perkins, D. L. Johnson, F. Peng, M. R. Penn, and M. T. Auer, "Patterns and impacts of inorganic tripton in Cayuga Lake," Hydrobiologia **482,** 137–150, doi: 10.1023/A.1021264415323 (2002).
41. S. W. Effler, C. M. Brooks, M. G. Perkins, N. K. Ohrazda, D. A. Matthews, D. L. Johnson, M. T. Auer, J. A. Bloomfield, and S. O. Quinn, "The effect of terrigenous inputs on spatial patterns of water quality indicators in South Lake, Lake Champlain," J. Great Lakes Res. **26,** 366–383 (2000).

42. S. W. Effler, M. G. Perkins, H. Greer, and D. L. Johnson, "Effect of 'whiting' on optical properties and turbidity in Owasco Lake, New York," Water Resour. Bull. **23,** 189–196 (1987).
43. C. T. Driscoll, S. W. Effler, and S. M. Doerr, "Changes in inorganic carbon chemistry and deposition of Onondaga Lake, New York," Environ. Sci. Technol. **28,** 1211–1218 (1994).
44. S. P. Madon, D. W. Schneider, J. A. Stoeckel, and R. E. Sparks, "Effects of inorganic sediment and food concentrations on energetic processes of the zebra mussel, *Dreissena polymorpha:* implications for growth in turbid rivers," Can. J. Fish. Aquat. Sci. **55,** 401–413 (1998).
45. S. W. Effler, R. K. Gelda, M. G. Perkins, and D. M. O'Donnell, "Modeling light attenuation, Secchi disk, and effects of tripton in Senaca River, New York, USA," J. Am. Water Resour. Assoc. **41,** 971–984 (2005).
46. C. Yin and D. L. Johnson, "An individual particle analysis and budget study of Onondaga Lake sediments," Limnol. Oceanogr. **29,** 1193–1201 (1984).
47. M. S. Twardowski, E. Boss, J. B. Macdonald, W. S. Pegau, A. H. Barnard, and J. R. V. Zaneveld, "A model for estimating bulk refractive index from the optical backscattering ratio and the implications for understanding particle composition in case I and case II waters," J. Geophys. Res., [Oceans] **106,** 14129–14142 (2001).
48. A. C. Holland and G. Gagne, "The scattering of polarized light by polydisperse systems of irregular particles," Appl. Opt. **9,** 1113–1121 (1970).
49. A. Mugnai and W. Wiscombe, "Scattering from nonspherical Chebyshev particles. 3. variability in angular scattering patterns," Appl. Opt. **28,** 3061–3073 (1989).
50. H. R. Gordon and T. Du, "Light scattering by nonspherical particles: application to coccoliths detached from *Emiliania huxleyi,*" Limnol. Oceanogr. **46,** 1438–1454 (2001).
51. H. Volten, J. F. de Haan, J. W. Hovenier, R. Schreurs, W. Vassen, A. G. Dekker, H. J. Hoogenboom, F. Charlton, and R. Wouts, "Laboratory measurements of angular distributions of light scattered by phytoplankton and silt," Limnol. Oceanogr. **43,** 1180–1197 (1998).
52. H. R. Gordon and O. B. Brown, "A theoretical model of light scattering by Sargasso Sea particulates," Limnol. Oceanogr. **17,** 826–832 (1972).
53. D. Stramski and S. B. Woźniak, "On the role of colloidal particles in light scattering in the ocean," Limnol. Oceanogr. **50,** 1581–1591 (2005).
54. C. E. Lambert, C. Jehanno, N. Silverberg, J. C. Brun-Cottan, and R. Chesselet, "Lognormal distributions of suspended particles in the open ocean," J. Mar. Res. **39,** 77–98 (1981).
55. D. Risović and M. Martinis, "A comparative analysis of sea-particle-size distribution models," Fiz. B **4,** 111–120 (1995).
56. H. Bader, "The hyperbolic distribution of particle sizes," J. Geophys. Res. **75,** 2822–2830 (1970).
57. J. M. Sullivan, M. S. Twardowski, P. L. Donaghay, and S. A. Freeman, "Use of optical scattering to discriminate particle types in coastal waters," Appl. Opt. **44,** 1667–1680 (2005).
58. F. P. Chavez, K. R. Buck, R. R. Bidigare, D. M. Karl, D. Hebel, M. Latasa, M. E. Ondrusek, L. Campbell, and J. Newton, "On the chlorophyll a retention properties of glass-fiber GF/F filters," Limnol. Oceanogr. **40,** 428–433 (1995).
59. R. W. Sheldon, "Size separation of marine seston by membrane and glass-fiber filters," Limnol. Oceanogr. **17,** 494–498 (1972).
60. R. H. Stavn and T. R. Keen, "Suspended minerogenic particle distributions in high-energy coastal environments: optical implications," J. Geophys. Res. **109,** C05005, doi:10.1029/2003JC002098 (2004).
61. A. L. Whitmire, E. Boss, T. J. Cowles, and W. S. Pegau, "Spectral variability of the particulate backscattering ratio," Opt. Express **15,** 7019–7031 (2007).
62. X. Zhang, M. Lewis, M. Lee, B. Johnson, and G. Korotaev, "The volume scattering function of natural bubble populations," Limnol. Oceanogr. **47,** 1273–1282 (2002).
63. D. M. Lavoie, "Computerized oceanic particle characterization using heavy metal staining, SEM, EDXS and image analysis," Deep-Sea Res., Part A **39,** 1655–1668 (1992).